Biophysical Chemistry 179 (2013) 12–25

Contents lists available at SciVerse ScienceDirect

Biophysical Chemistry

journal homepage: http://www.elsevier.com/locate/biophyschem

Heat-induced fibrillation of BclXL apoptotic repressor

Vikas Bhat [a], Max B. Olenick [a], Brett J. Schuchardt [a], David C. Mikles [a], Brian J. Deegan [a], Caleb B. McDonald [a], Kenneth L. Seldeen [a], Dmitry Kurouski [b], Mohd Hafeez Faridi [c], Mohammed M. Shareef [d], Vineet Gupta [c], Igor K. Lednev [b], Amjad Farooq [a,*]

[a] Department of Biochemistry & Molecular Biology, Leonard Miller School of Medicine, University of Miami, Miami, FL 33136, USA
[b] Department of Chemistry, University at Albany, SUNY, Albany, NY 12222, USA
[c] Division of Nephrology and Hypertension, Department of Medicine, Leonard Miller School of Medicine, University of Miami, Miami, FL 33136, USA
[d] Department of Radiation Oncology, Leonard Miller School of Medicine, University of Miami, Miami, FL 33136, USA

HIGHLIGHTS

- BclXL undergoes aggregation into amyloid-like fibrils at elevated temperature.
- Formation of such BclXL fibrils correlates with the decay of an α-helical fold into β-sheet.
- BclXL fibrils show no affinity toward BH3 ligands.
- BclXL fibrils are optimally primed for insertion into cardiolipin bicelles.

GRAPHICAL ABSTRACT

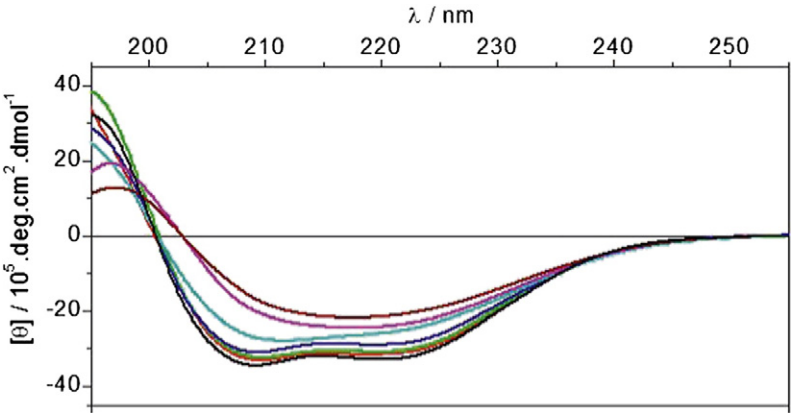

ARTICLE INFO

Article history:
Received 5 March 2013
Received in revised form 24 April 2013
Accepted 30 April 2013
Available online 7 May 2013

ABSTRACT

The BclXL apoptotic repressor bears the propensity to associate into megadalton oligomers in solution, particularly under acidic pH. Herein, using various biophysical methods, we analyze the effect of temperature on the oligomerization of BclXL. Our data show that BclXL undergoes irreversible aggregation and assembles into highly-ordered rope-like homogeneous fibrils with length in the order of mm and a diameter in the μm-range under elevated temperatures. Remarkably, the formation of such fibrils correlates with the decay of a largely α-helical fold into a predominantly β-sheet architecture of BclXL in a manner akin to the

Abbreviations: ALS, Analytical light scattering; ANS, 8-Anilinonaphthalene-1-sulfonate; Bad, Bcl2-associated death (promoter); Bak, Bcl2 (homologous) antagonist/killer; Bax, Bcl2-associated X (protein); Bcl2, B-cell lymphoma 2; BclXL, B-cell lymphoma extra large; BclXL_transTM, BclXL homodimer in which the TM domain of one monomer occupies the canonical hydrophobic groove within the other monomer and vice versa in a domain-swapped trans-fashion; BH1, Bcl2 homology 1 (domain); BH2, Bcl2 homology 2 (domain); BH3, Bcl2 homology 3 (domain); BH4, Bcl2 homology 4 (domain); Bid, BH3-interacting domain (death agonist); Bid_BH3, 20-mer peptide derived from the BH3 domain of Bid; CD, Circular dichroism; DHPC, 1,2-Dihexanoyl-*sn*-glycero-3-phosphocholine; DLS, Dynamic light scattering; FM, Fluorescence microscopy; ITC, Isothermal titration calorimetry; LIC, Ligation-independent cloning; MD, Molecular dynamics; MM, Molecular modeling; MOM, mitochondrial outer membrane; Myr, myricetin; SEC, Size-exclusion chromatography; SLS, Static light scattering; SSF, Steady-state fluorescence; ThT, Thioflavin T; TOCL, 1,1′,2,2′-Tetraoleoyl cardiolipin (1′,3′-bis[1,2-dioleoyl-*sn*-glycero-3-phospho]-*sn*-glycerol); TMAO, trimethylamine N-oxide.

* Corresponding author. Tel.: +1 305 243 2429; fax: +1 305 243 3955.
E-mail address: amjad@farooqlab.net (A. Farooq).

0301-4622/$ – see front matter
http://dx.doi.org/10.1016/j.bpc.2013.04.002

Keywords:
Amyloid fibrils
Kinetic trap
α–β structural transition
Irreversible aggregation
Membrane insertion

formation of amyloid fibrils. Further interrogation reveals that while BclXL fibrils formed under elevated temperatures show no observable affinity toward BH3 ligands, they appear to be optimally primed for insertion into cardiolipin bicelles. This salient observation strongly argues that BclXL fibrils likely represent an on-pathway intermediate for insertion into mitochondrial outer membrane during the onset of apoptosis. Collectively, our study sheds light on the propensity of BclXL to form amyloid-like fibrils with important consequences on its mechanism of action in gauging the apoptotic fate of cells in health and disease.

1. Introduction

Embryonic development and cellular homeostasis are heavily dependent on the concerted action of Bcl2 family of proteins in what has come to be known as apoptosis [1–8]. The Bcl2 proteins can be divided into three major groups with respect to their role in the regulation of apoptotic machinery: activators, effectors and repressors. Activators such as Bid and Bad belong to the BH3-only proteins, where BH3 is the Bcl2 homology 3 domain. Effectors such as Bax and Bak contain the BH3–BH1–BH2–TM modular architecture, where TM is the transmembrane domain located C-terminal to Bcl2 homology domains BH3, BH1 and BH2. Repressors such as Bcl2 and BclXL are usually characterized by the BH4–BH3–BH1–BH2–TM modular organization, with an additional N-terminal Bcl2 homology 4 domain.

How do Bcl2 proteins keep apoptosis in check? In a nutshell, the apoptotic fate, or the decision of a cell to live or die, is determined by the cellular ratio of activator, effector and repressor molecules [9,10]. In quiescent and healthy cells, the effectors are maintained in an inactive state via complexation with repressors. Upon receiving apoptotic cues, in the form of DNA damage and cellular stress, the activators are stimulated and compete with effectors for binding to the repressors and, in so doing, not only do they neutralize the anti-apoptotic action of repressors but also unleash the pro-apoptogenicity of effectors. The effectors subsequently initiate apoptotic cell death by virtue of their ability to insert into the mitochondrial outer membrane (MOM) resulting in the formation of mitochondrial pores in a manner akin to the insertion of bacterial toxins such as colicins and diphtheria [11–15]. This leads to the release of apoptogenic factors such as cytochrome c and Smac/Diablo from mitochondria into the cytosol. Subsequently, rising levels of apoptogenic factors in the cytosol switch on aspartate-specific proteases termed caspases, which in turn, demolish the cellular architecture by cleavage of proteins culminating in total cellular destruction.

While there is a general consensus that hetero-association between various members of the Bcl2 family represents a defining event in the decision of a cell to live or die, the biophysical basis of such protein–protein interactions remains hitherto poorly characterized and, in particular, our limited knowledge on the ability of Bcl2 proteins to undergo homo-association into higher-order oligomers and aggregates leaves much to be desired in our quest to further our understanding of apoptosis at molecular level. Toward this goal, our previous studies have shown that BclXL apoptotic repressor bears the propensity to associate into megadalton oligomers in solution, particularly under acidic pH, and that such aggregation is largely mediated by the C-terminal transmembrane (TM) domain [16,17]. Importantly, a truncated construct of BclXL lacking the C-terminal TM domain, was recently shown to form amyloid-like fibrils under elevated temperatures [18]. This salient observation invokes a key role of thermal energy in driving the aggregation of BclXL. In an effort to further explore the effect of elevated temperature, we have conducted here detailed biophysical analysis on the propensity of full-length BclXL, harboring the C-terminal TM domain, to undergo oligomerization. It is important to note here that temperature is one of the key physical factors that governs the ability of many proteins to associate into higher-order oligomers. Additionally, elevated temperature should also serve as a mimicry for cellular stress and thus may shed light on how cellular homeostasis may regulate the oligomerization of this key apoptotic regulator.

2. Materials and methods

2.1. Sample preparation

Full-length human BclXL (residues 1–233) was cloned into pET30 bacterial expression vector with an N-terminal His-tag using Novagen LIC technology, expressed in Escherichia coli BL21*(DE3) bacterial strain (Invitrogen) and purified on a Ni-NTA affinity column using standard procedures as described previously [16,17]. Protein concentration was determined by the fluorescence-based Quant-It assay (Invitrogen) and spectrophotometrically on the basis of an extinction coefficient of 47,440 M^{-1} cm^{-1} calculated for the full-length BclXL using the online software ProtParam at ExPasy Server [19]. Results from both methods were in an excellent agreement. The 20-mer peptide spanning residues 81–100 corresponding to the BH3 domain within human Bid (H_2N-DIIRNIARHLAQVGDSMDRS-COOH), herein referred to as Bid_BH3, was commercially obtained from GenScript Corporation. The peptide concentration was measured gravimetrically. Mixed TOCL/DHPC bicelles were prepared at a final concentration of 30 mM, at TOCL to DHPC molar ratio of 1:4, by stirring for 2 h at 37 °C. For biophysical experiments described below, all protein, peptide and bicelle samples were prepared in 50 mM Sodium phosphate buffer containing 100 mM NaCl (except for CD measurements) at pH 8.0. Except for transient measurements, samples of BclXL were pre-incubated overnight at various temperatures ranging from 20 °C to 80 °C prior to each experiment. All measurements were repeated at least three times.

2.2. Molecular modeling

Molecular modeling (MM) was employed to build a domain-swapped structural model of BclXL homodimer, herein referred to as BclXL_transTM, using the MODELLER software [20,21]. Briefly, in the BclXL_transTM structural model, the TM domain of one monomer occupies the canonical hydrophobic groove within the other monomer and vice versa in a domain-swapped trans-fashion as described earlier [16,17]. The structural model was rendered using RIBBONS [22].

2.3. Molecular dynamics

Molecular dynamics (MD) simulations were performed with the GROMACS software [23,24] using the integrated OPLS-AA force field [25,26]. Briefly, the BclXL_transTM structural model was centered within a cubic box, hydrated using the extended simple point charge (SPC/E) water model [27,28], and the ionic strength of solution was set to 100 mM with NaCl. The hydrated structure was energy-minimized with the steepest descent algorithm prior to equilibration under the NPT ensemble conditions, wherein the number of atoms (N), pressure (P) and temperature (T) within the system were kept constant. The Particle-Mesh Ewald (PME) method was employed to compute long-range electrostatic interactions with a 10 Å cut-off [29] and the Linear Constraint Solver (LINCS) algorithm to restrain bond lengths [30]. All MD simulations were performed under periodic boundary conditions (PBC) at 20 °C, 40 °C, 60 °C and 80 °C using the leap-frog integrator with a time step of 2 fs. For the final MD production runs, data were collected every 100 ps over a time scale of 100 ns. All simulations were run on a Linux workstation using parallel processors at the High

Performance Computing facility within the Center for Computational Science of the University of Miami.

2.4. Analytical light scattering

Analytical light scattering (ALS) experiments were conducted on a Wyatt miniDAWN TREOS triple-angle static light scattering detector and Wyatt QELS dynamic light scattering detector coupled in-line with a Wyatt Optilab rEX differential refractive index detector and interfaced to a Hiload Superdex 200 size-exclusion chromatography column under the control of a GE Akta FPLC system within a chromatography refrigerator at 10 °C. Briefly, pre-heated samples of 10 μM BclXL at various temperatures ranging from 20 °C to 80 °C were loaded onto the column at a flow rate of 1 ml/min and the data were automatically acquired using the ASTRA software. The angular- and concentration-dependence of static light scattering (SLS) intensity of BclXL resolved in the flow mode was measured by the Wyatt miniDAWN TREOS detector equipped with three scattering angles positioned at 42°, 90° and 138°. The time- and concentration-dependence of dynamic light scattering (DLS) intensity fluctuation of BclXL resolved in the flow mode was measured by the Wyatt QELS detector positioned at 90° with respect to the incident laser beam. Hydrodynamic parameters M_w (weighted-average molar mass), M_n (number-average molar mass), R_g (weighted-average radius of gyration) and R_h (weighted-average hydrodynamic radius) associated with solution behavior of BclXL were determined by the treatment of SLS data to Zimm model and by non-linear least-squares fit of DLS data to an autocorrelation function as described earlier [16,17]. It should be noted that, in both the SLS and DLS measurements, protein concentration (c) along the elution profile of BclXL was automatically quantified in the ASTRA software from the change in refractive index (Δn) with respect to the solvent as measured by the Wyatt Optilab rEX detector using the following relationship:

$$c = (\Delta n)/(dn/dc) \quad (1)$$

where dn/dc is the refractive index increment of the protein in solution.

2.5. Circular dichroism

Circular dichroism (CD) measurements were conducted on a thermostatically-controlled Jasco J-815 spectrometer at 25 °C. For far-UV steady-state measurements, experiments were conducted on pre-heated samples of 10 μM BclXL alone, pre-equilibrated with 100 μM Bid_BH3 peptide, or pre-equilibrated with 2 mM TOCL/DHPC bicelles at various temperatures ranging from 20 °C to 80 °C and data were collected using a quartz cuvette with a 2-mm pathlength in the 195–255 nm wavelength range. For near-UV steady-state measurements, experiments were conducted on pre-heated samples of 50 μM BclXL alone at various temperatures ranging from 20 °C to 80 °C and data were collected using a quartz cuvette with a 10-mm pathlength in the 255-315 nm wavelength range. In each case, a slit bandwidth of 2 nm was used and data were recorded at a scan rate of 10 nm/min. All spectral data were normalized against reference spectra to remove the background contribution of buffer. Each spectral data set represents an average of four scans acquired at 0.1 nm intervals. All data were converted to mean ellipticity, [θ], as a function of wavelength (λ) of electromagnetic radiation using the equation:

$$[\theta] = \left[\left(10^5 \Delta\theta\right)/cl\right] \text{ deg.cm}^2\text{.dmol}^{-1} \quad (2)$$

where Δθ is the observed ellipticity in mdeg, c is the protein concentration in μM and l is the cuvette pathlength in cm. For far-UV transient measurements, freshly purified samples of 10 μM BclXL alone, pre-equilibrated with 100 μM Bid_BH3 peptide, or pre-equilibrated with 1 mM TOCL/DHPC bicelles at 20 °C were placed in a quartz cuvette with a 2-mm pathlength and the change in spectral intensity at 222 nm, $[\theta]_{222}$, was monitored over three consecutive temperature steps (herein denoted Steps I–III) as a function of time for 90 min: in Step I, the temperature was ramped up from 20 °C to 80 °C at a ramp rate of 2 °C/min over the time period 0–30 min; in Step II, the temperature was held constant at 80 °C over the time period 31–60 min; in Step III, the temperature was ramped down from 80 °C to 20 °C at a ramp rate of 2 °C/min over the time period 61–90 min.

2.6. Steady-state fluorescence

Steady-state fluorescence (SSF) spectra were collected on a thermostatically-controlled Jasco FP-6300 spectrofluorimeter using a quartz cuvette with a 10-mm pathlength at 25 °C. Briefly, experiments were conducted on pre-heated samples of 10 μM BclXL pre-equilibrated with 100 μM ANS, 10 μM BclXL pre-equilibrated with 10 μM ThT, 10 μM BclXL pre-equilibrated with 10 μM ThT and 100 μM Myr, or 10 μM lysozyme pre-equilibrated with 10 μM ThT (as a positive control) at various temperatures ranging from 20 °C to 80 °C. For ANS fluorescence, the excitation wavelength was 375 nm and emission was acquired over the 400–700 nm wavelength range. For ThT fluorescence, the excitation wavelength was 420 nm and emission was acquired over the 430–650 nm wavelength range. All data were recorded using a 2.5-nm bandwidth for both excitation and emission. Data were normalized against reference spectra to remove background contribution of protein and buffer. Fluorescence enhancement (E) of ANS or ThT in the presence of BclXL at each incubation temperature was calculated from the following equation:

$$E = [(\Phi - \Phi_o)/\Phi_o] \times 100\% \quad (3)$$

where Φ is the fluorescence yield of ANS or ThT in the presence of BclXL and Φ_o is the fluorescence yield of ANS or ThT alone at corresponding incubation temperature. Fluorescence yield (Φ) is defined as the area integrated under the corresponding emission spectra.

2.7. Isothermal titration calorimetry

Isothermal titration calorimetry (ITC) experiments were performed on a Microcal VP-ITC instrument at 25 °C. Briefly, experiments were conducted to probe the binding of Bid_BH3 peptide and mixed TOCL/DHPC bicelles to pre-heated samples of 50 μM BclXL at various temperatures ranging from 20 °C to 80 °C. For peptide binding, experiments were initiated by injecting 25 × 10 μl aliquots of 1 mM of Bid_BH3 peptide from the syringe into the calorimetric cell containing 1.8 ml of pre-heated samples of 50 μM BclXL. For membrane insertion, experiments were initiated by injecting 25 × 10 μl aliquots of pre-heated samples of 50 μM BclXL from the syringe into the calorimetric cell containing 1.8 ml of 2 mM of TOCL/DHPC. In each case, the change in thermal power as a function of each injection was automatically recorded using the ORIGIN software and the raw data were further processed to yield binding isotherms of heat release per injection either as a function of molar ratio of peptide to BclXL or as a function of molar ratio of BclXL to bicelles. The heats of mixing and dilution were subtracted from the heats of peptide binding or membrane insertion per injection by carrying out a control experiment in which the same buffer in the calorimetric cell was either titrated against the Bid_BH3 peptide or BclXL in an identical manner. The apparent equilibrium dissociation constant (K_d) and the enthalpic change (ΔH) associated with peptide binding to BclXL or membrane insertion of BclXL were determined from the non-linear least-squares fit of data to a one-site binding model as described previously [31,17]. The binding free energy change (ΔG) was calculated from the following expression:

$$\Delta G = RT\ln K_d \quad (4)$$

where R is the universal molar gas constant (1.99 cal/K/mol) and T is the absolute temperature. The entropic contribution (TΔS) to the free energy of binding was calculated from the relationship:

$$T\Delta S = \Delta H - \Delta G \quad (5)$$

where ΔH and ΔG are as defined above.

2.8. Fluorescence microscopy

Fluorescence microscopy (FM) experiments were conducted on a Leica DMI6000 microscope with 10× objective. All images were analyzed and processed using Leica LAS-AF software. Data were collected on pre-heated samples of 25 μM BclXL alone, pre-equilibrated with 250 μM Bid_BH3 peptide, or pre-equilibrated with 2 mM TOCL/DHPC bicelles at various incubation temperatures ranging from 20 °C to 80 °C. Prior to imaging, each sample was stained with 25 μM ThT and mounted onto a glass slide.

3. Results and discussion

3.1. BclXL harbors intrinsic propensity to aggregate

On the basis of previous X-ray crystallographic and molecular modeling analysis [32,33,16,17], the 3D structural topology of BclXL is characterized by a central predominantly hydrophobic α-helical hairpin "dagger" (α5 and α6) surrounded by a "cloak" comprised of six amphipathic α-helices (α1–α4 and α7–α8) of varying lengths. The so-called "canonical hydrophobic groove", that serves as the docking site for the BH3 domain of activators and effectors, is formed by the juxtaposition of α2–α5 helices. Additionally, BclXL is decorated with a C-terminal hydrophobic α-helix termed α9, or more commonly the TM domain, which is believed to facilitate localization of BclXL to MOM upon apoptotic induction [34–36].

Importantly, we have previously shown that BclXL displays the propensity to oligomerize in solution and that such oligomerization is driven by the intermolecular binding of its C-terminal TM domain to the canonical hydrophobic groove in a domain-swapped trans-fashion [16,17], whereby the TM domain of one monomer occupies the canonical hydrophobic groove within the other monomer and vice versa in what we refer to as the BclXL_transTM conformation (Fig. 1a). We further postulated that such homodimerization could in turn drive the association of BclXL into higher-order megadalton aggregates.

In light of the knowledge that a wide range of proteins share the ability to aggregate into amyloid-like fibrils under environmental stresses such as acidic pH and elevated temperatures [37–40], we also analyzed the intrinsic propensity of BclXL to aggregate into fibrils using aggregation predictors such as AMYLPRED [41] and AGGRESCAN [42]. As shown in Fig. 1b, our in silico analysis reveals that BclXL indeed harbors intrinsic propensity to aggregate and that the residues that drive such aggregation primarily reside within the BH1 (α4–α5) and TM (α9) domains. While the involvement of BH1 domain in promoting the aggregation is somewhat surprising, the role of TM domain is in full agreement with our previous studies demonstrating that its deletion abolishes the association of BclXL into larger aggregates [16,17].

3.2. Thermal motions appear to destabilize the structural architecture of BclXL

Our previous studies have shown that the BclXL apoptotic repressor bears the propensity to associate into megadalton aggregates in solution, particularly under acidic pH [16,17]. To understand the extent to which elevated temperature may also contribute to such aggregation, we conducted MD simulations on the BclXL_transTM dimeric conformation over tens of nanoseconds at various temperatures (Fig. 2). As shown in Fig. 2a, the MD trajectories reveal that while BclXL reaches

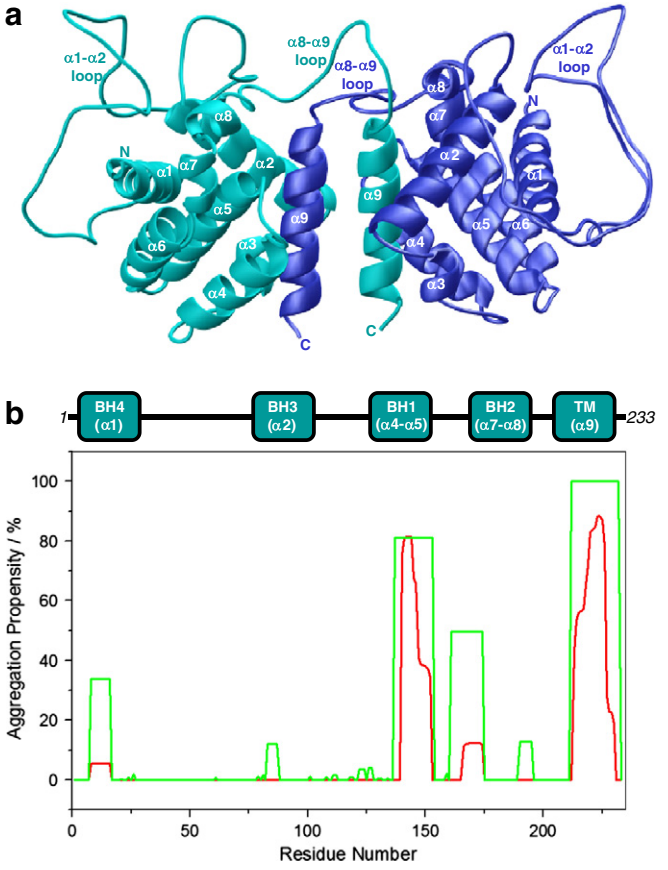

Fig. 1. In silico analysis of BclXL. (a) A structural model of a dimeric conformation of BclXL (BclXL_transTM), where the TM domain of one monomer (cyan) occupies the canonical hydrophobic groove within the other monomer (blue) and vice versa in a domain-swapped trans-fashion swapping as described earlier [16,17]. (b) Plots showing the propensity of BclXL to aggregate into amyloid-like fibrils as predicted by AMYLPRED (red) and AGGRESCAN (green). Note that the BH4–BH3–BH1–BH2–TM modular architecture of BclXL is overlaid for direct correlation of aggregation propensity to specific domains within BclXL.

structural equilibrium after about 20 ns under all temperatures, its stability is compromised under elevated temperatures. Thus, while the root mean square deviation (RMSD) of BclXL at structural equilibrium fluctuates around 8 Å at low temperatures (20 °C and 40 °C), it rises to around 12 Å under elevated temperatures (60 °C and 80 °C). This strongly argues that the poor structural stability of BclXL due to enhanced thermal motions under elevated temperatures may account for its ability to associate into higher-order aggregates.

An alternative means to assess mobility and stability of macromolecular complexes is through an assessment of the root mean square fluctuation (RMSF) of specific atoms over the course of MD simulation. Fig. 2b provides such analysis for the backbone atoms of each residue within BclXL. The RMSF analysis shows that while a majority of residues within BclXL appear to be well-ordered under all temperatures, the residues within the α1–α2 loop experience rapid fluctuations which are particularly more exaggerated at 20 °C but become more widespread at 80 °C. Accordingly, the change in motional properties of residues within the α1–α2 loop under elevated temperatures could trigger the association of BclXL into larger aggregates. It is noteworthy that the deletion of the α1–α2 loop in BclXL augments its anti-apoptogenicity and that the suppressive effect of α1–α2 loop is relieved by its post-translational phosphorylation [43]. In light of this observation, we believe that the intrinsic flexibility of the α1–α2 loop may be a driving force for the aggregation of BclXL through favorable entropic contributions and that such intermolecular association most likely compromises its anti-apoptotic action. Interestingly, our in silico analysis presented

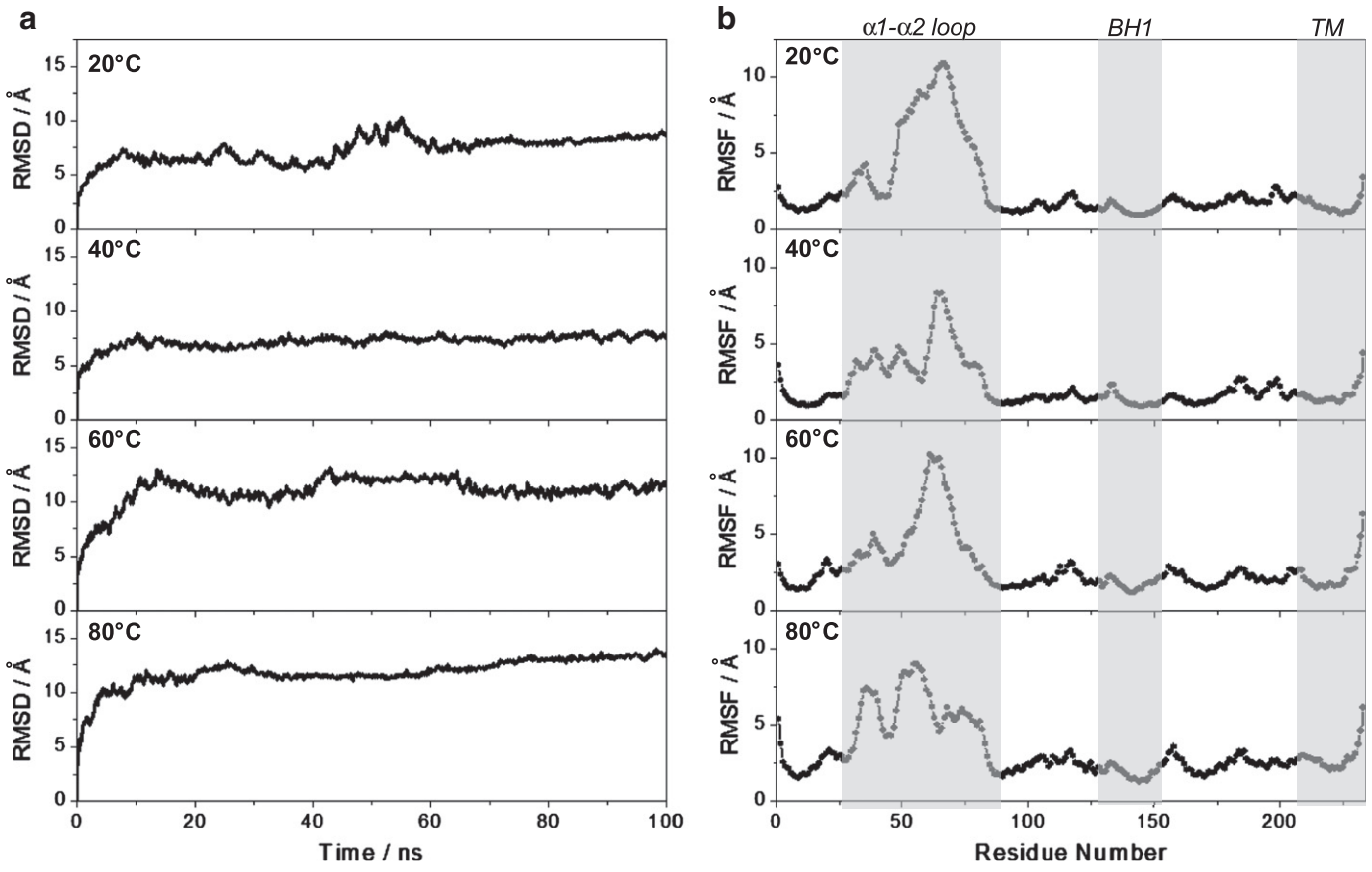

Fig. 2. MD analysis of BclXL_transTM conformation at various temperatures as indicated. (a) Root mean square deviation (RMSD) of backbone atoms (N, Cα and C) within each simulated structure relative to the initial modeled structure of BclXL_transTM as a function of simulation time. (b) Root mean square fluctuation (RMSF) of backbone atoms (N, Cα and C) averaged over the entire course of corresponding MD trajectory of the modeled structure of BclXL_transTM as a function of residue number. Note that the shaded vertical rectangular boxes indicate the residue boundaries of the α1–α2 loop as well as the BH1 and TM domains.

above reveals that the major determinants of the propensity of BclXL to aggregate most likely reside within the BH1 and TM domains in lieu of the α1–α2 loop (Fig. 1b). However, residues within the BH1 and TM domains show no observable change in their backbone dynamics in response to changes in temperature. This likely suggests that the molecular origin of factors promoting the aggregation of BclXL is highly complex and may not necessarily be governed by changes in thermal motions. Nevertheless, our MD simulations provide molecular insights into the effect of temperature on the motional properties of BclXL.

3.3. Elevated temperature shifts the equilibrium of BclXL into megadalton aggregates

To directly test the extent to which temperature may promote the association of BclXL into larger aggregates, we conducted ALS analysis on pre-heated samples of BclXL at various temperatures ranging from 20 °C to 80 °C and quantified physical parameters accompanying its solution behavior from the first principles of hydrodynamics without any assumptions (Fig. 3 and Table 1). Our data indicate that BclXL exists in various associative conformations at 20 °C, ranging from monomer (31kD) and dimer (62kD) to higher-order oligomers, herein referred to as multimer (~400kD) and polymer (~4000kD). At 40 °C, the dimer and multimer conformers appear to shift in the direction of the polymeric conformation. Remarkably, under elevated temperatures (60 °C and 80 °C), BclXL appears to largely exist in a large aggregate that we refer to herein as megamer. This strongly suggests that elevated temperature facilitates association of BclXL into megadalton aggregates. Notably, the truncation of C-terminal TM domain completely abolished oligomerization of BclXL under low temperatures (20 °C and 40 °C), while only small aggregates were observed under elevated temperatures (60 °C and 80 °C). These observations are in general agreement with previous studies showing that a C-terminally truncated construct of BclXL forms amyloid-like fibrils under elevated temperatures [18]. However, our data presented above implicate a key role of TM domain in driving the intermolecular association of BclXL into large aggregates in agreement with our previous studies [16,17].

In an attempt to gain insights into the conformational heterogeneity of the oligomeric species of BclXL, we also determined the M_w/M_n and R_g/R_h ratios from our hydrodynamic data (Table 1). It should be noted that while the M_w/M_n ratio provides a measure of the macromolecular polydispersity, the R_g/R_h ratio sheds light on the overall macromolecular shape. Our data suggest that while the higher-order oligomers (multimer and polymer) of BclXL display some degree of polydispersity ($M_w/M_n > 1.05$) under all temperatures, the monomeric and dimeric forms of BclXL are predominantly monodisperse ($M_w/M_n < 1.05$). Strikingly, BclXL not only exclusively exists as a megadalton oligomer under elevated temperatures (60 °C and 80 °C) but it also surprisingly appears to be highly monodisperse ($M_w/M_n < 1.05$). Additionally, the higher-order oligomers (multimer and polymer) of BclXL most likely adopt an elongated rod-like shape ($R_g/R_h > 1.05$) in lieu of a more spherical or compact structure. Consistent with these observations, the megameric species observed under elevated temperatures (60 °C and 80 °C) also seem to adopt an highly elongated rod-like architecture ($R_g/R_h > 2$) with a radius of gyration of ~100 nm, arguing that it may bear the propensity to assemble into fibrils of up to hundreds of nm in length in a manner akin to amyloid fibrils. It should be noted that the actual size of BclXL aggregates observed under elevated temperatures is likely to be much larger due to the fact that the various hydrodynamic

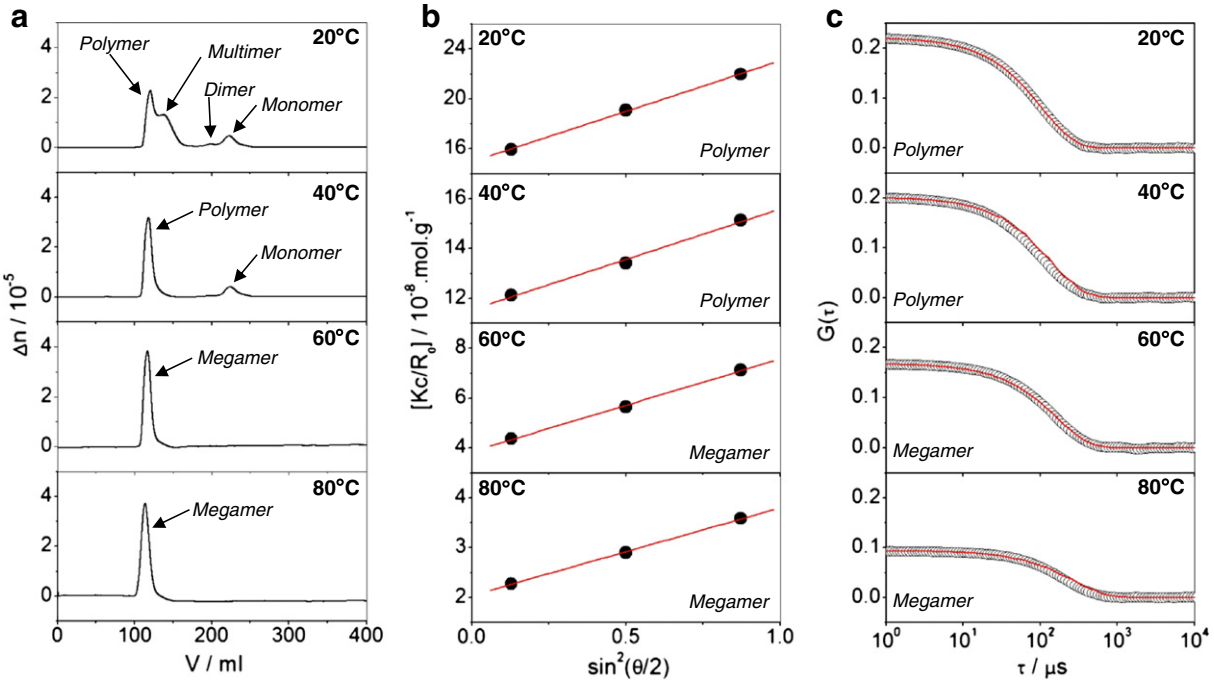

Fig. 3. ALS analysis of BclXL pre-heated overnight at various temperatures as indicated. (a) Elution profiles of BclXL as monitored by the differential refractive index (Δn) plotted as a function of elution volume (V). (b) Partial Zimm plots obtained for the oligomeric species of BclXL as indicated from analytical SLS measurements. Note that the red solid lines through the data points represent linear fits. (c) Autocorrelation function plots obtained for various oligomeric species of BclXL as indicated from analytical DLS measurements. Note that the red solid lines represent non-linear least squares fit of data to an autocorrelation function as described earlier [16,17].

parameters reported here exceed the upper limit of detection of ALS. Additionally, hydrodynamic properties of such BclXL aggregates are most likely underestimated here due to the filtration of protein samples prior to ALS analysis, implying that larger aggregates most likely never reach the ALS detectors. We also note that our ALS analysis of BclXL in the presence of TOCL/DHPC bicelles—as a model for MOM—was complicated by the fact that the scattering of light by bicelles swamped the protein signal, thereby rendering it very difficult to analyze the effect of bicelles on BclXL aggregates.

3.4. BclXL undergoes structural transition at elevated temperature

It is well-documented that many proteins that aggregate into amyloid-like fibrils adopt cross β-sheet structure combined with the loss of globular fold [44–48]. Thus, we wondered whether the ability of BclXL to associate into large aggregates under elevated temperatures is also coupled to such structural changes. To address this question, we carried out CD analysis on BclXL pre-heated overnight at various temperatures ranging from 20 °C to 80 °C (Fig. 4). Our far-UV CD analysis shows that BclXL displays spectral features characteristic of an α-helical fold with bands centered around 208 nm and 222 nm at lower temperatures (Fig. 4a, top panel). Remarkably, under elevated temperatures, the α-helical spectral features of BclXL disappear at the expense of appearance of a new band around 216 nm, which is characteristic of β-sheet architecture. These salient observations suggest that BclXL undergoes structural transition from a predominantly α-helical fold to a largely β-sheet conformation.

To monitor how elevated temperature affects tertiary structure of BclXL, we next conducted near-UV CD analysis in a similar manner (Fig. 4b, top panel). Unsurprisingly, BclXL displays spectral features in the near-UV region characteristic of a well-folded globular protein with bands emanating from the chiral environment surrounding aromatic residues such as phenylalanine (258 nm), tyrosine (282 nm) and tryptophan (293 nm) at lower temperatures. Consistent with our far-UV CD analysis presented above, these bands either largely disappear or become substantially attenuated at elevated temperatures. This is evidence that BclXL aggregates lose their native tertiary structure and adopt a more fibrillar conformation that presumably lacks a well-defined tertiary structure under elevated temperatures.

Importantly, the lack of a single isosbestic point in both the far-UV and near-UV spectra recorded for BclXL at various temperatures strongly argues that the conversion of an α-helical fold into β-sheet architecture

Table 1
Hydrodynamic parameters for BclXL pre-incubated at the indicated temperatures.

	Associativity	M_w/kD	M_n/kD	M_w/M_n	R_g/Å	R_h/Å	R_g/R_h	P/%
20 °C	Monomer	34 ± 3	33 ± 3	1.02 ± 0.01	ND	25 ± 2	ND	14
	Dimer	59 ± 4	57 ± 4	1.03 ± 0.01	ND	45 ± 3	ND	3
	Multimer	374 ± 23	353 ± 15	1.06 ± 0.02	101 ± 9	87 ± 3	1.25 ± 0.02	39
	Polymer	3787 ± 242	3227 ± 185	1.16 ± 0.04	248 ± 31	184 ± 9	1.33 ± 0.15	44
40 °C	Monomer	30 ± 2	29 ± 2	1.03 ± 0.01	ND	28 ± 4	ND	20
	Polymer	8729 ± 797	7660 ± 948	1.15 ± 0.05	407 ± 20	223 ± 15	1.82 ± 0.16	80
60 °C	Megamer	24,895 ± 1463	24,145 ± 1039	1.04 ± 0.02	598 ± 28	274 ± 24	2.17 ± 0.10	100
80 °C	Megamer	61,010 ± 7624	60,730 ± 7741	1.01 ± 0.01	709 ± 86	341 ± 48	2.08 ± 0.17	100

All parameters were obtained from ALS measurements. The population (P) of each species, as estimated from the integration of corresponding peak in the elution profile (Fig. 3a), is provided in the right-most column. Note that the calculated molar mass of recombinant full-length BclXL from amino acid sequence alone is 31kD. Errors were calculated from at least three independent measurements. All errors are given to one standard deviation. Note that the R_g parameter could not be determined (ND) for various species due to their lack of angular-dependence of scattered light.

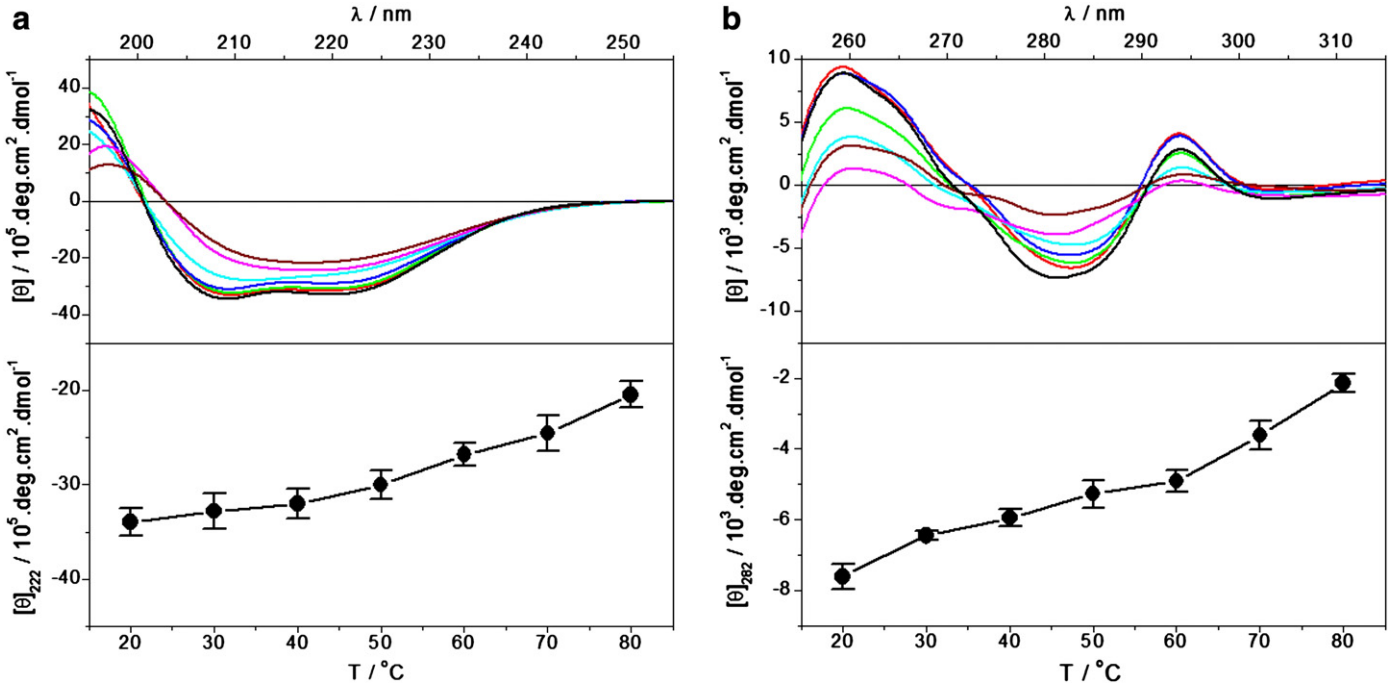

Fig. 4. Steady-state CD analysis of BclXL pre-heated overnight at various temperatures. (a) Far-UV spectra of BclXL (top panel) and the dependence of mean ellipticity at 222 nm, $[\theta]_{222}$, on temperature (bottom panel). (b) Near-UV spectra of BclXL (top panel) and the dependence of mean ellipticity at 282 nm, $[\theta]_{282}$, on temperature (bottom panel). In the top panels, the spectra shown were recorded at 20 °C (black), 30 °C (red), 40 °C (green), 50 °C (blue), 60 °C (cyan), 70 °C (magenta) and 80 °C (brown). In the bottom panels, the data points are connected with a solid line for clarity. The error bars were calculated from three independent measurements to one standard deviation.

occurs via at least one intermediate step (Fig. 4a and b, top panels). This view is further corroborated by the observation that the dependence of spectral intensities at 222 nm (monitoring secondary structural changes) and 282 nm (monitoring tertiary structural changes) displays multiphasic behavior with increasing temperature in lieu of a linear relationship (Fig. 4a and b, bottom panels). Taken

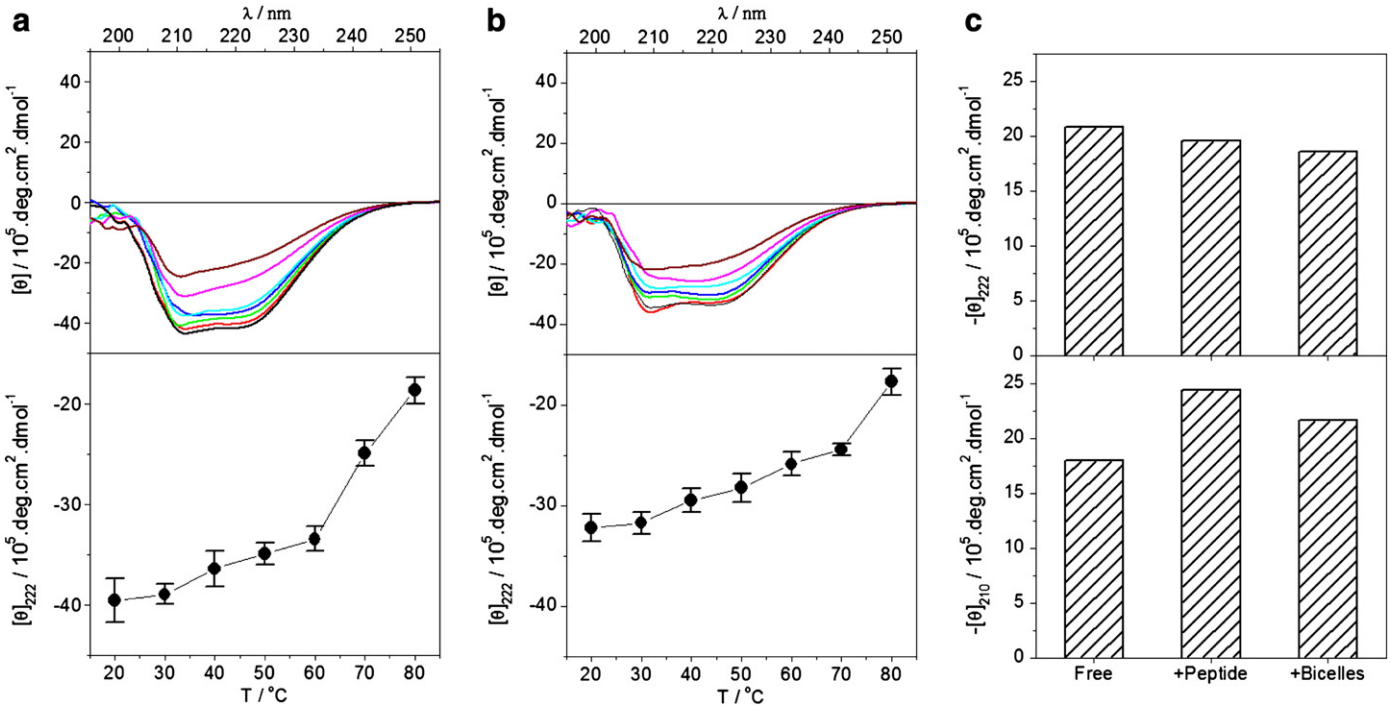

Fig. 5. Steady-state CD analysis of BclXL pre-equilibrated with Bid_BH3 peptide (a) or TOCL/DHPC bicelles (b) overnight at various temperatures (T). (a) Far-UV spectra of BclXL pre-equilibrated with Bid_BH3 peptide (top panel) and the dependence of mean ellipticity at 222 nm, $[\theta]_{222}$, on temperature (bottom panel). (b) Far-UV spectra of BclXL pre-equilibrated with TOCL/DHPC bicelles (top panel) and the dependence of mean ellipticity at 222 nm, $[\theta]_{222}$, on temperature (bottom panel). In the top panels in (a) and (b), the spectra shown were recorded at 20 °C (black), 30 °C (red), 40 °C (green), 50 °C (blue), 60 °C (cyan), 70 °C (magenta) and 80 °C (brown). In the bottom panels in (a) and (b), the data points are connected with a solid line for clarity. The error bars were calculated from three independent measurements to one standard deviation. (c) Comparison of mean ellipticity at 222 nm (top panel), $[\theta]_{222}$, and 210 nm (bottom panel), $[\theta]_{210}$, for BclXL alone (Free), BclXL pre-equilibrated with Bid_BH3 peptide (+Peptide), or BclXL pre-equilibrated with TOCL/DHPC bicelles (+Bicelles) overnight at 80 °C.

together, our far-UV and near-UV CD data strongly suggest that BclXL aggregates observed under elevated temperatures most likely adopt a cross β-sheet structure characteristic of amyloid-like fibrils.

3.5. BclXL undergoes distinct structural transition upon interaction with BH3 ligand and MOM mimetic

To understand how BH3 ligands and MOM mimetics modulate the extent to which the BclXL interconverts from an α-helical fold to a β-sheet conformation, we conducted far-UV CD analysis on BclXL pre-equilibrated overnight either with a 20-mer BH3 peptide derived from Bid activator (Bid_BH3) or mixed TOCL/DHPC bicelles—used here as a model for MOM—at various temperatures ranging from 20 °C to 80 °C (Fig. 5). Remarkably, our analysis reveals that while BclXL adopts a predominantly α-helical fold with minima centered around 210 nm and to a lesser extent at 222 nm in the presence of Bid_BH3 peptide and TOCL/DHPC bicelles at 20 °C (Fig. 5a and b), it undergoes structural transition in which the minima around 210 nm and 222 nm are more or less preserved but experience a loss in spectral intensity at elevated temperatures. This suggests strongly that the peptide and the bicelles induce a structural transition within BclXL that is distinct from that observed for BclXL alone at elevated temperatures. We interpret such structural transition from a partial loss of α-helical fold to a coiled-coil conformation in sharp contrast to the β-sheet architecture observed for BclXL alone at elevated temperatures. Such differences in the structural transition are further highlighted by the differential changes observed in the ellipticity at 222 nm as a function of temperature for BclXL alone (Fig. 4a, bottom panel) versus those observed in the presence of Bid_BH3 peptide (Fig. 5a, bottom panel) and TOCL/DHPC bicelles (Fig. 5b, bottom panel). Notably, comparison of mean ellipticity at 210 nm and 222 nm for BclXL alone, BclXL pre-equilibrated with Bid_BH3 peptide, and BclXL pre-equilibrated with TOCL/DHPC bicelles overnight at 80 °C further corroborates the notion that BclXL undergoes distinct structural changes at elevated temperatures depending on whether it is heated alone in solution or in the presence of its ligands (Fig. 5c).

3.6. Aggregation of BclXL under elevated temperature represents a kinetic trap

Our steady-state CD data presented above suggest that the α–β structural transition of BclXL alone, in the presence of Bid_BH3 peptide or TOCL/DHPC bicelles at elevated temperatures overnight is an irreversible process in that the protein aggregates retain their integrity and β-sheet structure when cooled down to a temperature of 25 °C (Figs. 4 and 5). In an attempt to directly gauge the kinetics and reversibility of temperature-induced aggregates of BclXL on a shorter time scale, we next transiently monitored the far-UV CD spectral intensity at 222 nm, $[\theta]_{222}$, of BclXL alone, pre-equilibrated with Bid_BH3 peptide, or pre-equilibrated with mixed TOCL/DHPC bicelles at 20 °C as a function of temperature in the 20–80 °C range over a time period of 90 min (Fig. 6).

Consistent with our far-UV CD data presented above, $[\theta]_{222}$ of BclXL alone increases with increasing temperature from 20 °C to 80 °C (Fig. 6a), implying that BclXL undergoes α–β transition under elevated temperatures. Importantly, $[\theta]_{222}$ of BclXL alone exquisitely plateaus out as the temperature reaches a constant value of 80 °C and the resulting plateau is unaffected upon the reversal of the temperature from 80 °C to 20 °C. This salient observation further corroborates the notion that the temperature-induced formation of BclXL aggregates is an irreversible process that results in a kinetic trap. Interestingly, when BclXL is pre-equilibrated with Bid_BH3 peptide, $[\theta]_{222}$ shows no change as a function of time (Fig. 6b), implying that the binding of BH3 ligands to BclXL slows down the aggregation of BclXL. Finally, pre-equilibration of BclXL with TOCL/DHPC bicelles does not appear to dramatically affect the aggregation of BclXL as monitored by changes in $[\theta]_{222}$ (Fig. 6c).

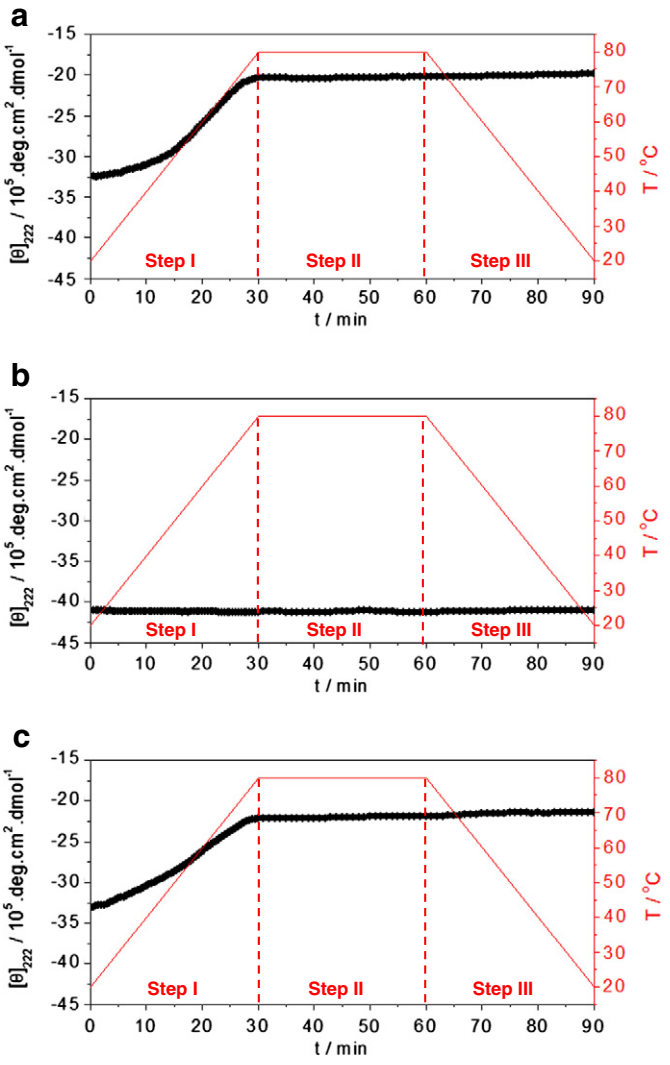

Fig. 6. Transient CD analysis of BclXL alone (a), pre-equilibrated with Bid_BH3 peptide (b), or pre-equilibrated with TOCL/DHPC bicelles at 20 °C (c). Briefly, changes in mean ellipticity at 222 nm, $[\theta]_{222}$, were monitored for each sample over three consecutive temperature steps (herein denoted Steps I–III) as a function of time for 90 min: in Step I, the temperature was ramped up from 20 °C to 80 °C at a ramp rate of 2 °C/min over the time period 0–30 min; in Step II, the temperature was held constant at 80 °C over the time period 31–60 min; in Step III, the temperature was ramped down from 80 °C to 20 °C at a ramp rate of 2 °C/min over the time period 61–90 min. In each panel, the red solid line shows the change in temperature (T) as a function of time (t) and the three temperature steps are demarcated by vertical dashed lines.

3.7. BclXL harbors structural features characteristics of amyloid fibrils under elevated temperature

In light of the knowledge that many proteins that aggregate into amyloid-like fibrils adopt cross β-sheet structure with exposed hydrophobic surfaces [44–48], we next analyzed the ability of BclXL to aggregate under various temperatures ranging from 20 °C to 80 °C using fluorescent hydrophobic dyes in combination with SSF (Fig. 7). It is well-documented that the fluorescence of hydrophobic dyes such as ANS and ThT undergoes enhancement upon binding to the canonical cross β-sheet topology and the exposed hydrophobic surfaces characteristic of amyloid-like fibrils [49–53]. Consistent with this notion, our analysis reveals that while ANS fluorescence undergoes nearly two-fold enhancement when BclXL is pre-heated to 80 °C relative to incubation at 20 °C (Fig. 7a), ThT experiences close to an order of

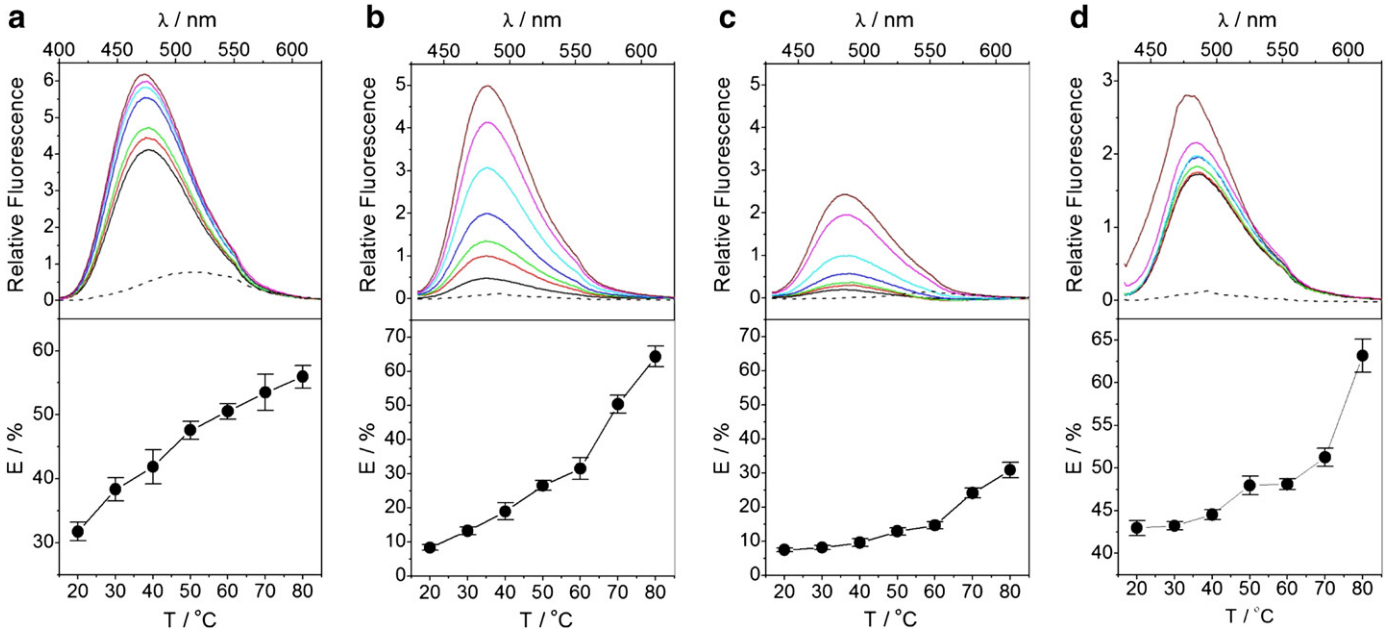

Fig. 7. SSF analysis of BclXL pre-heated overnight at various temperatures. (a) Fluorescence spectra of ANS in the presence of BclXL (top panel) and the dependence of ANS fluorescence enhancement (E) on temperature (bottom panel). (b) Fluorescence spectra of ThT in the presence of BclXL (top panel) and the dependence of ThT fluorescence enhancement (E) on temperature (bottom panel). (c) Fluorescence spectra of ThT in the presence of BclXL pre-equilibrated with Myr (top panel) and the dependence of ThT fluorescence enhancement (E) on temperature (bottom panel). (d) Fluorescence spectra of ThT in the presence of lysozyme (top panel) and the dependence of ThT fluorescence enhancement (E) on temperature (bottom panel). In the top panels, the fluorescence spectra shown were recorded at 20 °C (black), 30 °C (red), 40 °C (green), 50 °C (blue), 60 °C (cyan), 70 °C (magenta) and 80 °C (brown). Note that the dashed lines indicate the background fluorescence spectra of ANS (a), ThT (b and d) and ThT pre-equilibrated with Myr (c) in buffer alone. In the bottom panels, the data points are connected with a solid line for clarity. The error bars were calculated from three independent measurements to one standard deviation.

magnitude fluorescence enhancement (Fig. 7b). We note that while the emission of ANS and ThT occurs maximally around 500–515 nm in water, it appears to be blue-shifted to around 475 nm upon binding to BclXL. This is further evidence for the exposure of hydrophobic surfaces in BclXL, which apparently becomes more exaggerated under elevated temperatures. Importantly, polyphenols such as Myr have been shown to destabilize amyloid fibrils [54]. We wondered whether Myr may also have a similar effect on the fibrillar aggregates observed for BclXL under elevated temperatures. Indeed, when BclXL is pre-equilibrated with ThT in the presence of Myr prior to heating at various temperatures, the fluorescence enhancement of ThT is substantially reduced under elevated temperatures (Fig. 7c). It is also important to note that the dependence of fluorescence enhancement of ANS and ThT displays multiphasic behavior with increasing temperature in lieu of a linear trend (Fig. 7a–c, bottom panels). As noted above, this implies that the decay of a α-helical fold into β-sheet architecture occurs via at least one intermediate step upon the heating of BclXL.

To further corroborate the notion that the enhancement of hydrophobic dyes such as ThT upon binding to BclXL correlates with the formation of amyloid fibrils, we also used lysozyme as a positive control. Notably, it is widely-documented that lysozyme forms amyloid fibrils at elevated temperatures [55–57]. Consistent with this knowledge, our analysis shows that ThT experiences close to two-fold fluorescence enhancement when lysozyme is pre-heated to 80 °C relative to incubation at 20 °C in a manner akin to that observed for BclXL (Fig. 7d). However, the fact that the ThT fluorescence enhancement observed for lysozyme is much less than that noted for BclXL under similar conditions suggests that BclXL fibrils are likely to be much larger in size than those of lysozyme. It is noteworthy that SSF analysis of BclXL in the presence of TOCL/DHPC bicelles was complicated by the fact that the hydrophobic dyes ANS and ThT strongly bound to the bicelles and, in so doing, swamped the fluorescence changes due to their binding to BclXL alone under various conditions. Accordingly, such binding overlap prevented us from conducting any reliable measurements on BclXL in the presence of bicelles. Nonetheless, our data presented above strongly support the credence that elevated temperatures promote the aggregation of BclXL into amyloid-like fibrils.

3.8. Aggregation compromises the binding of BclXL to BH3 ligands

During apoptosis, BclXL exerts its suppressive effect by virtue of its ability to recruit the BH3 domains of apoptotic effectors such as Bax and Bak and, in so doing, neutralizes their pro-apoptotic function [9,10]. However, our data presented above suggest that BclXL undergoes structural transition from a largely α-helical fold into a cross β-sheet structure characteristic of amyloid-like fibrils under elevated temperatures. Accordingly, we would predict that the formation of such fibrillar aggregates is likely to be directly coupled to the loss of ligand binding to BclXL—since the above-mentioned structural transition would compromise the integrity of the canonical hydrophobic groove within BclXL required for ligand binding.

To test this hypothesis, we conducted ITC analysis for the binding of Bid_BH3 peptide to BclXL pre-incubated at various temperatures ranging from 20 °C to 80 °C (Fig. 8 and Table 2). Our data show that the binding of Bid_BH3 peptide to BclXL becomes progressively attenuated by more than an order of magnitude as the incubation temperature is raised from 20 °C to 60 °C and becomes completely abolished when BclXL is pre-heated to 80 °C. It should be noted here that the stoichiometries for the binding of Bid_BH3 peptide to BclXL were fixed to unity during the fit of the ITC data at all temperatures to allow for the loss of an incompetent fraction of protein unable to bind ligand. However, when the stoichiometries were allowed to float, there was little or negligible change in the values of the binding constants or the underlying thermodynamic parameters as reported in Table 2.

Interestingly, the loss of ligand binding with increasing incubation temperature correlates with both the loss of favorable enthalpic change and unfavorable entropy, implying that BclXL undergoes more "ordered" structure at elevated temperatures in agreement with its propensity to aggregate into amyloid-like fibrils. Collectively, our data suggest that BclXL loses the ability to recognize BH3 ligands upon

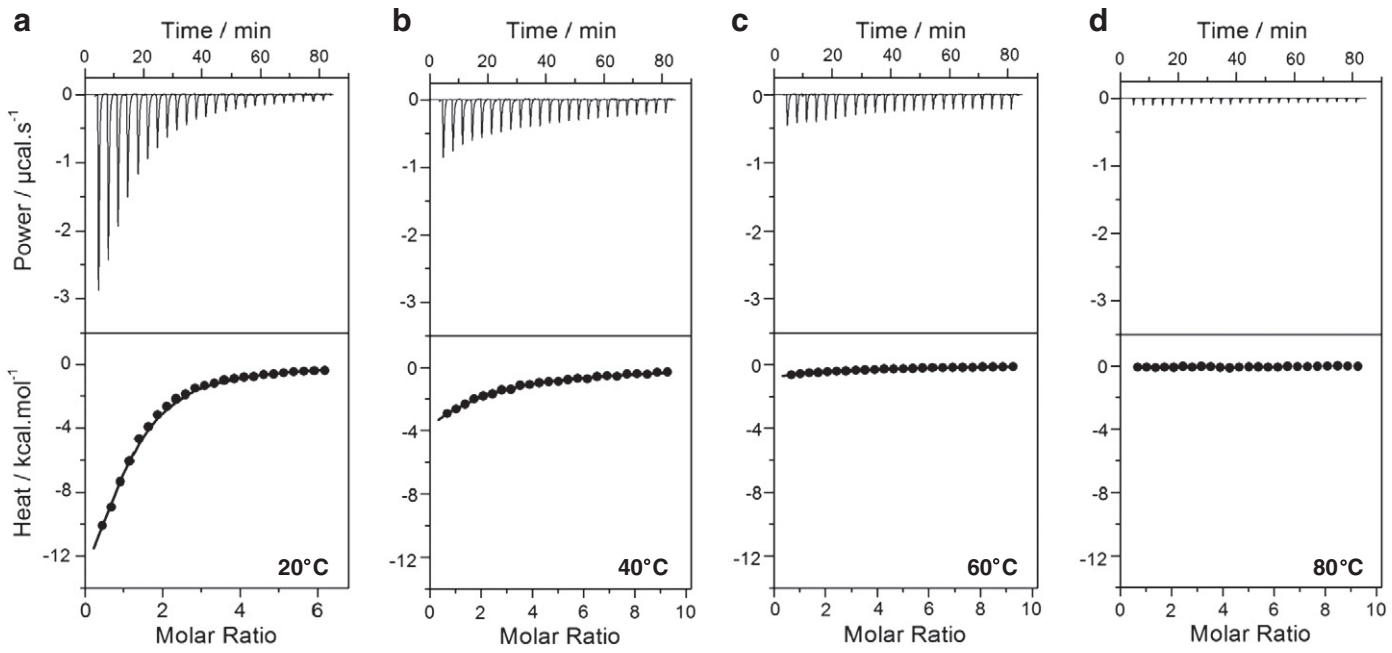

Fig. 8. ITC analysis for the binding of Bid_BH3 peptide to BclXL pre-heated overnight at 20 °C (a), 40 °C (b), 60 °C (c) and 80 °C (d). The upper panels show raw ITC data expressed as change in thermal power with respect to time over the period of titration. In the lower panels, change in molar heat is expressed as a function of molar ratio of Bid_BH3 peptide to BclXL. The solid lines in the lower panels show non-linear least squares fit of data to a one-site binding model using the ORIGIN software as described earlier [16,17].

aggregation and such behavior should also be expected to result in the loss of its anti-apoptotic function.

3.9. Aggregation promotes the insertion of BclXL into lipid bicelles

In light of the knowledge that the amyloid-like fibrils bear the potential to permeabilize cellular membranes and lipid bilayers [58–62], we next wondered whether the fibrillar aggregates observed here under elevated temperatures may also represent a facilitated route for the entry of BclXL into MOM. To test this hypothesis, we analyzed the binding of BclXL pre-incubated at various temperatures ranging from 20 °C to 80 °C to mixed TOCL/DHPC bicelles using ITC (Fig. 9 and Table 3). Remarkably, our analysis reveals that BclXL binds to TOCL/DHPC bicelles, used here as a model for MOM, only when pre-heated to temperatures of 40 °C and above. Importantly, titration of BclXL aggregates into the calorimetric cell containing the buffer alone resulted in little or negligible change in thermal power (Fig. 9a–d), implying that the observed heat change is not due to dissociation of BclXL aggregates but rather results from a direct and specific interaction between BclXL and bicelles. We interpret such BclXL–lipid interaction in terms of the insertion of BclXL into bicelles in light of the knowledge that BclXL not only contains a C-terminal TM domain that spontaneously inserts into synthetic membranes but it also localizes to MOM during the onset of apoptosis [35,63–65].

It should be noted that the stoichiometries for the binding of BclXL to TOCL/DHPC bicelles were typically around 0.001 at all temperatures. This implies that the binding of one molecule of BclXL requires about 1000 molecules of lipids and, in so doing, this gives rise to rather low protein–lipid stochiometries observed here. Notwithstanding these limitations, our data suggest that BclXL fibrils represent an on-pathway intermediate state primed for insertion into MOM with important consequences on cellular physiology. Could BclXL harbor functional duality in its ability to act as anti-apoptotic under one state (globular) and pro-apoptotic (fibrillar) under another? In this regard, it is interesting to note that caspase-induced N-terminal cleavage of BclXL within the cellular milieu renders it pro-apoptotic [66–68]. Thus, it is conceivable that the propensity of BclXL to aggregate into fibrils may represent an alternative mechanism to trigger its pro-apoptotic action.

Importantly, we also note that while the binding of BclXL pre-heated to temperatures of 37 °C and above to TOCL/DHPC bicelles occurs with similar affinities, the underlying thermodynamics governing this membrane–protein interaction bear substantial differences. Thus, for example, while the favorable enthalpy change accompanying this membrane–protein interaction more than doubles in magnitude from an incubation temperature of 37 °C to 80 °C, exactly the opposite trend is observed in the case of unfavorable entropic contribution such that it compensates any net gain in the free energy and hence the binding affinity. This trend is due to the phenomenon of enthalpy–entropy compensation that widely governs the thermodynamic behavior of macromolecular interactions.

Table 2
Thermodynamic parameters for the binding of Bid_BH3 peptide to BclXL pre-incubated at the indicated temperatures.

	K_d/µM	ΔH/kcal·mol^{-1}	TΔS/kcal·mol^{-1}	ΔG/kcal·mol^{-1}
20 °C	8.90 ± 1.71	−19.11 ± 0.63	−12.15 ± 0.52	−6.90 ± 0.11
25 °C	10.90 ± 2.41	−18.75 ± 0.19	−11.96 ± 0.06	−6.78 ± 0.13
37 °C	38.13 ± 7.95	−16.03 ± 0.20	−9.99 ± 0.32	−6.04 ± 0.12
40 °C	48.39 ± 9.51	−14.26 ± 0.61	−8.37 ± 0.49	−5.89 ± 0.12
60 °C	147.51 ± 30.28	−5.54 ± 0.11	−0.31 ± 0.02	−5.23 ± 0.13
80 °C	NB	NB	NB	NB

All parameters were obtained from ITC measurements. The stoichiometries for the binding of Bid_BH3 peptide to BclXL were fixed to unity at all temperatures to allow for the loss of an incompetent fraction of protein unable to bind ligand. Errors were calculated from at least three independent measurements. All errors are given to one standard deviation. NB indicates no binding observed.

3.10. Aggregation results in the formation of highly-ordered rope-like homogeneous fibrils of BclXL

To understand the morphological and structural features of fibrillar aggregates of BclXL and how they may be modulated by ligand binding and membrane insertion, we conducted FM analysis on samples of BclXL pre-heated at various temperatures ranging from 20 °C to 80 °C and pre-stained with ThT (Fig. 10). Our data show that while no observable fibrils are detected at lower temperatures (20 °C and 40 °C), BclXL

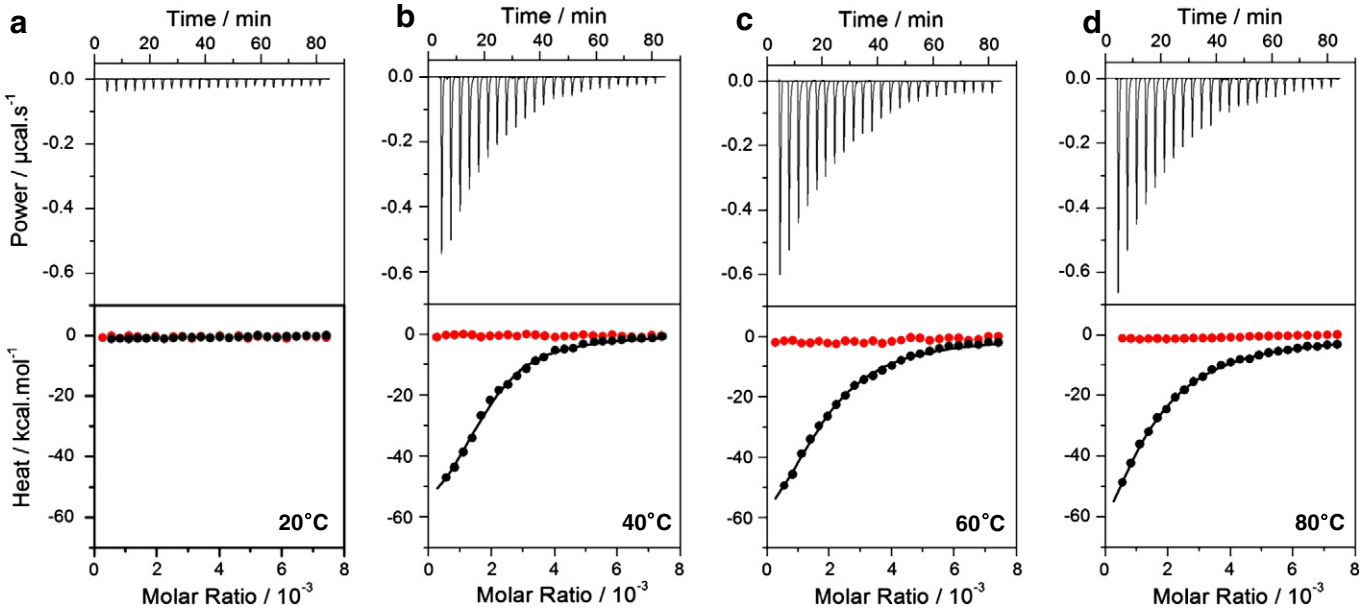

Fig. 9. ITC analysis for the binding of mixed TOCL/DHPC bicelles to BclXL pre-heated overnight at 20 °C (a), 40 °C (b), 60 °C (c) and 80 °C (d). The upper panels show raw ITC data expressed as change in thermal power with respect to time over the period of titration. In the lower panels, change in molar heat is expressed as a function of molar ratio of BclXL to bicelles (●). Titration of BclXL pre-heated overnight at 20 °C (a), 40 °C (b), 60 °C (c) and 80 °C (d) into buffer alone is also shown as a control (●). The solid lines in the lower panels show non-linear least squares fit of data to a one-site binding model using the ORIGIN software as described earlier [16,17].

forms highly-ordered rope-like homogeneous fibrils at higher temperatures (60 °C and 80 °C) with length in the order of mm and a diameter in the μm-range (Fig. 10a). It should be noted that while electron microscopy analysis on BcXL revealed the formation of small non-fibrillar aggregates at lower temperatures (20 °C and 40 °C) in agreement with our ALS analysis (Fig. 3), the rather large fibrils observed at higher temperatures (60 °C and 80 °C) were better suited for FM analysis.

Importantly, amyloid-like fibrils hitherto reported for other proteins typically tend to be less than μm in length and nm in diameter [69–71,37–40,72]. The fact that BclXL fibrils observed here under elevated temperatures are three orders of magnitude larger in size than anything ever reported before is highly surprising and of particular significance. Interestingly, while the rope-like morphological features of BclXL fibrils under elevated temperatures were by and large unaffected in the presence of Bid_BH3 peptide (Fig. 10b), the addition of mixed TOCL/DHPC bicelles apparently abolished their formation (Fig. 10c). Of particular note here is the observation that while the lack of ability of Bid_BH3 peptide to halt the formation of BclXL fibrils is consistent with our far-UV CD data (Fig. 5a), the apparent loss of fibrillar architecture upon interaction of BclXL with TOCL/DHPC bicelles is highly surprising (Fig. 5b). In order to reconcile the discrepancy between our FM and CD data, we reason that while the insertion of BclXL fibrils into TOCL/DHPC bicelles appears to be coupled with its α–β structural transition as observed in our far-UV CD (Fig. 5b), the resulting β-sheet structure within mixed bicelles is unlikely to bear the hallmarks of a fibrillar architecture in agreement with our FM analysis (Fig. 10c).

Taken together, these data demonstrate that while BH3 ligands may not affect its ability to form fibrillar aggregates, the insertion of BclXL into MOM likely is highly preferred over its ability to undergo fibrillation. This salient observation further corroborates the notion that the BclXL fibrils may serve as an on-pathway intermediate for membrane insertion.

Table 3
Thermodynamic parameters for the binding of mixed TOCL/DHPC bicelles to BclXL pre-incubated at the indicated temperatures.

	K_d/μM	ΔH/kcal·mol^{-1}	TΔS/kcal·mol^{-1}	ΔG/kcal·mol^{-1}
20 °C	NB	NB	NB	NB
25 °C	NB	NB	NB	NB
37 °C	4.1 ± 0.84	−44.0 ± 1.41	−36.63 ± 1.29	−7.36 ± 0.12
40 °C	2.8 ± 0.42	−59.5 ± 2.12	−51.9 ± 2.03	−7.58 ± 0.09
60 °C	2.5 ± 0.49	−79.0 ± 2.82	−71.3 ± 2.70	−7.66 ± 0.12
80 °C	2.7 ± 0.35	−115.0 ± 3.32	−107.4 ± 3.10	−7.62 ± 0.07

All parameters were obtained from ITC measurements. The stoichiometries for the binding of BclXL to TOCL/DHPC bicelles were typically around 0.001 (one molecule of BclXL bound per 1000 molecules of bicelles) at all temperatures. Errors were calculated from at least three independent measurements. All errors are given to one standard deviation. NB indicates no binding observed.

4. Conclusions

Although the central role of Bcl2 proteins in orchestrating apoptosis has been known for more than two decades [73–77], the underlying mechanisms remain far from understood. Previous studies have shown that truncated constructs of BclXL apoptotic repressor display the propensity to homodimerize in solution [78,66,79]. These observations are further supported by studies conducted within live mammalian cells [80,81]. More recently, a truncated construct of BclXL lacking the C-terminal TM domain, was shown to form amyloid-like fibrils under elevated temperatures [18]. However, biophysical work from our laboratory on purified recombinant full-length BclXL to apparent homogeneity is beginning to provide new insights into the role of C-terminal TM domain in driving the aggregation of this key apoptotic repressor into higher-order oligomers [16,17]. In a continuing theme, we have examined here the effect of temperature on the propensity of full-length BclXL to undergo such oligomerization.

The conventional wisdom in molecular biophysics is that heating proteins results in their irreversible and amorphous aggregation due to the loss of intramolecular forces such as hydrogen bonding, ion pairing and van der Waals contacts required for the integrity of native fold. In this study, we have demonstrated that the BclXL apoptotic repressor undergoes transformation to another "ordered" secondary structure characteristic of amyloid-like fibrils instead of amorphous aggregation when subjected to elevated temperatures. Amyloid fibrils typically display a characteristic cross-β sheet structure, which is essentially comprised of an array of β-sheets running perpendicularly along the fibril axis [69–72]. It is important to note that a wide range of

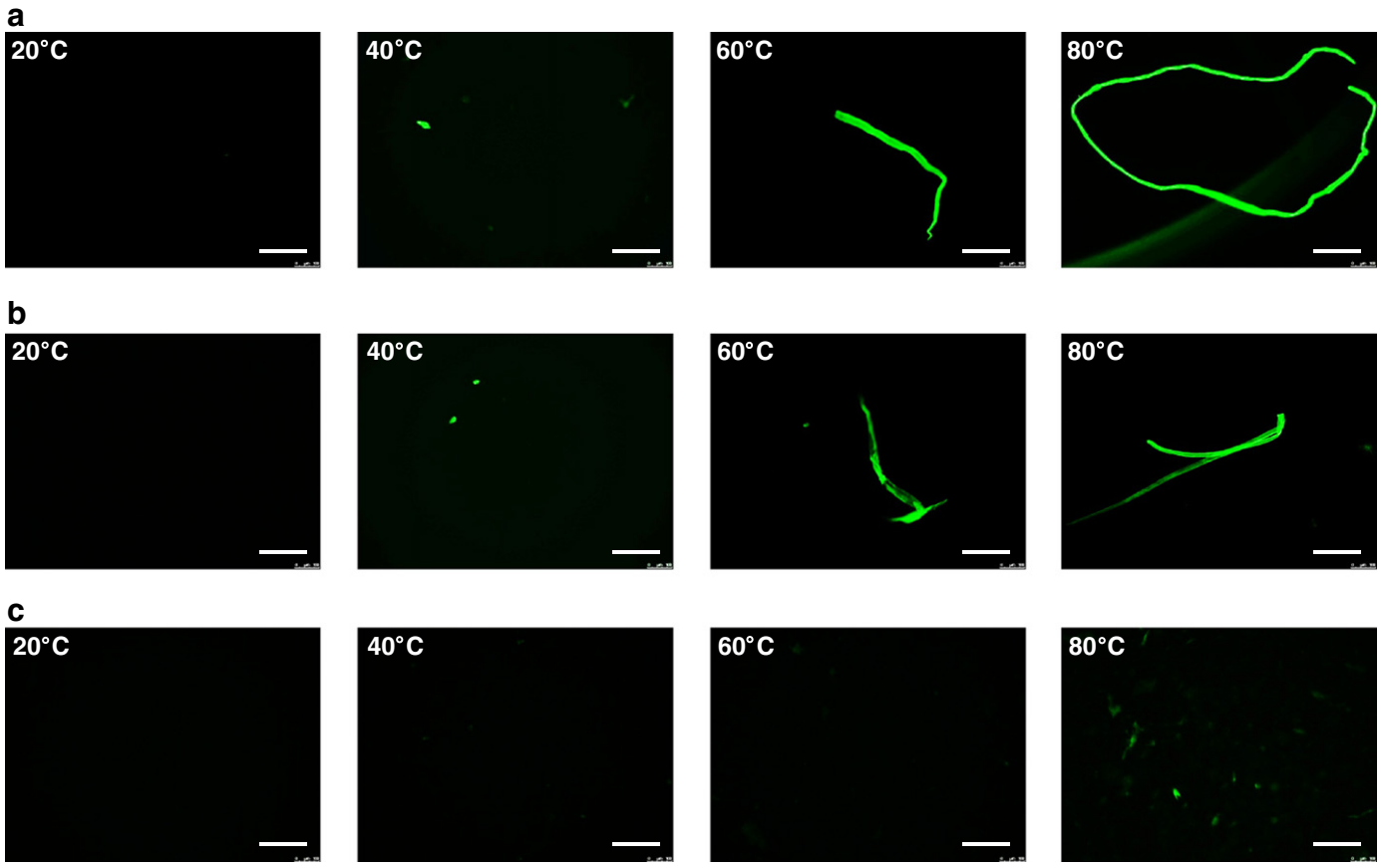

Fig. 10. FM micrographs of BclXL alone (a), pre-equilibrated with Bid_BH3 peptide (b), and pre-equilibrated with mixed TOCL/DHPC bicelles (c) at various temperatures overnight. All images were taken after pre-staining of BclXL with ThT. The scale bar represents 200 μm.

proteins are known to aggregate under environmental stresses such as acidic pH and elevated temperatures into amyloid fibrils [37–40]. In particular, the deposition of amyloid-like fibrils is believed to play a central role in the pathogenesis of many diseases such as α-synuclein in Parkinson's disease, tau protein in Alzheimer's disease, prion in bovine spongiform encephalopathy, and huntingtin in Huntington's disease [82–85]. Strikingly, while amyloid fibrils implicated in such diseases typically tend to be μm in length, the ability of BclXL to form elongated fibrils up to mm in length is highly surprising. Interestingly, the structure-inducing osmolyte TMAO has been previously shown to induce the formation of rope-like tropoelastin fibrils comparable in size to those observed here for BclXL [86]. Whether TMAO may exert a similar effect on BclXL under ambient temperature remains to be seen.

It is telling that a truncated construct of BclXL devoid of the C-terminal TM domain has also been shown to form amyloid-like fibrils, albeit much smaller than those observed here, under elevated temperatures [18]. This suggests that while TM domain likely facilitates the aggregation of BclXL into amyloid-like fibrils, other regions also harbor intrinsic aggregation propensity in agreement with our in silico analysis presented here. While our study does not demonstrate the physiological relevance of the ability of BclXL to aggregate into fibrils, the fact that such fibrils appear to be primed for insertion into cardiolipin bicelles provides an interesting scenario. Thus, under cellular stress mimicking elevated temperatures, the BclXL fibrillar aggregates may insert into MOM resulting in the formation of mitochondrial pores, thereby leading to the release of apoptogenic factors from mitochondria into the cytosol and triggering the induction of apoptosis in a manner akin to Bax and Bak effectors [9,10]. Alternatively, the formation of rope-like fibrils under cellular stress may enable BclXL to physically damage the intracellular membranes and/or interfere with the ability of actin cytoskeleton to orchestrate cellular signaling involved in a diverse array for processes central to the maintenance of a healthy environment.

Could BclXL have a functional duality in that it may antagonize apoptotic machinery in quiescent healthy cells but drive apoptosis under cellular stress? This notion gains further momentum in light of the fact that amyloid-like fibrils share the ability to permeabilize cellular membranes and lipid bilayers, implying that this may represent the primary toxic mechanism of amyloid pathogenesis [58–62]. More importantly, lysozyme fibrils have been shown to induce apoptotic cell death by virtue of their ability to induce membrane damage [87]. Finally, caspase-induced cleavage of α1–α2 loop of BclXL within mammalian cells has been shown to convert BclXL from being a pro-survival to pro-apoptotic factor [88]. Thus, the daring possibility that BclXL fibrils may also promote apoptosis warrants further inquiry in vivo. While this work is beyond the scope of our current study, it is set to take center stage in our future efforts directed at unraveling the mysteries of this key apoptotic player.

Acknowledgments

We are deeply indebted to the Sylvia Daunert group for the use of its Jasco J-815 spectropolarimeter. This work was supported by the National Institutes of Health Grants R01-GM083897 (to AF), R01-AG033719 (to IKL), and R01-DK084195 (to VG), and funds from the USylvester Braman Family Breast Cancer Institute (to AF). MMS is supported by the Department of Defense Grant# W91ZSQ1295N677. CBM is a recipient of a postdoctoral fellowship from the National Institutes of Health (Award# T32-CA119929).

References

[1] J.M. Adams, S. Cory, The Bcl-2 protein family: arbiters of cell survival, Science 281 (1998) 1322–1326.
[2] A. Gross, J.M. McDonnell, S.J. Korsmeyer, BCL-2 family members and the mitochondria in apoptosis, Genes & Development 13 (1999) 1899–1911.
[3] S.J. Korsmeyer, BCL-2 gene family and the regulation of programmed cell death, Cancer Research 59 (1999) 1693s–1700s.
[4] T. Kuwana, D.D. Newmeyer, Bcl-2-family proteins and the role of mitochondria in apoptosis, Current Opinion in Cell Biology 15 (2003) 691–699.
[5] R.J. Youle, A. Strasser, The BCL-2 protein family: opposing activities that mediate cell death, Nature Reviews Molecular Cell Biology 9 (2008) 47–59.
[6] G. Dewson, R.M. Kluck, Mechanisms by which Bak and Bax permeabilise mitochondria during apoptosis, Journal of Cell Science 122 (2009) 2801–2808.
[7] J.E. Chipuk, T. Moldoveanu, F. Llambi, M.J. Parsons, D.R. Green, The BCL-2 family reunion, Molecular Cell 37 (2010) 299–310.
[8] L.M. Dejean, S.Y. Ryu, S. Martinez-Caballero, O. Teijido, P.M. Peixoto, K.W. Kinnally, MAC and Bcl-2 family proteins conspire in a deadly plot, Biochimica et Biophysica Acta 1797 (2010) 1231–1238.
[9] J.E. Chipuk, J.C. Fisher, C.P. Dillon, R.W. Kriwacki, T. Kuwana, D.R. Green, Mechanism of apoptosis induction by inhibition of the anti-apoptotic BCL-2 proteins, Proceedings of the National Academy of Sciences of the United States of America 105 (2008) 20327–20332.
[10] J.E. Chipuk, D.R. Green, How do BCL-2 proteins induce mitochondrial outer membrane permeabilization? Trends in Cell Biology 18 (2008) 157–164.
[11] F.G. van der Goot, J.M. Gonzalez-Manas, J.H. Lakey, F. Pattus, A 'molten-globule' membrane-insertion intermediate of the pore-forming domain of colicin A, Nature 354 (1991) 408–410.
[12] E. London, Diphtheria toxin: membrane interaction and membrane translocation, Biochimica et Biophysica Acta 1113 (1992) 25–51.
[13] J.H. Lakey, F.G. van der Goot, F. Pattus, All in the family: the toxic activity of pore-forming colicins, Toxicology 87 (1994) 85–108.
[14] S.L. Schendel, M. Montal, J.C. Reed, Bcl-2 family proteins as ion-channels, Cell Death and Differentiation 5 (1998) 372–380.
[15] S.D. Zakharov, W.A. Cramer, Colicin crystal structures: pathways and mechanisms for colicin insertion into membranes, Biochimica et Biophysica Acta 1565 (2002) 333–346.
[16] V. Bhat, D. Kurouski, M.B. Olenick, C.B. McDonald, D.C. Mikles, B.J. Deegan, K.L. Seldeen, I.K. Lednev, A. Farooq, Acidic pH promotes oligomerization and membrane insertion of the BclXL apoptotic repressor, Archives of Biochemistry and Biophysics 528 (2012) 32–44.
[17] V. Bhat, C.B. McDonald, D.C. Mikles, B.J. Deegan, K.L. Seldeen, M.L. Bates, A. Farooq, Ligand Binding and Membrane Insertion Compete with Oligomerization of the BclXL Apoptotic Repressor, Journal of Molecular Biology 416 (2012) 57–77.
[18] A. Chenal, C. Vendrely, H. Vitrac, J.C. Karst, A. Gonneaud, C.E. Blanchet, S. Pichard, E. Garcia, B. Salin, P. Catty, D. Gillet, N. Hussy, C. Marquette, C. Almunia, V. Forge, Amyloid fibrils formed by the programmed cell death regulator Bcl-xL, Journal of Molecular Biology 415 (2012) 584–599.
[19] E. Gasteiger, C. Hoogland, A. Gattiker, S. Duvaud, M.R. Wilkins, R.D. Appel, A. Bairoch, Protein Identification and Analysis Tools on the ExPASy Server, in: J.M. Walker (Ed.), The Proteomics Protocols Handbook, Humana Press, Totowa, New Jersey, USA, 2005, pp. 571–607.
[20] R. Koradi, M. Billeter, K. Wuthrich, MOLMOL: a program for display and analysis of macromolecular structures, Journal of Molecular Graphics 14 (1996) 51–55.
[21] M.A. Marti-Renom, A.C. Stuart, A. Fiser, R. Sanchez, F. Melo, A. Sali, Comparative Protein Structure Modeling of Genes and Genomes, Annual Review of Biophysics and Biomolecular Structure 29 (2000) 291–325.
[22] M. Carson, Ribbons 2.0, Journal of Applied Crystallography 24 (1991) 958–961.
[23] D. Van Der Spoel, E. Lindahl, B. Hess, G. Groenhof, A.E. Mark, H.J. Berendsen, GROMACS: fast, flexible, and free, Journal of Computational Chemistry 26 (2005) 1701–1718.
[24] B. Hess, GROMACS 4: algorithms for highly efficient, load-balanced, and scalable molecular simulation, Journal of Chemical Theory and Computation 4 (2008) 435–447.
[25] W.L. Jorgensen, J. Tirado-Rives, The OPLS force field for proteins: energy minimizations for crystals of cyclic peptides and crambin, Journal of the American Chemical Society 110 (1988) 1657–1666.
[26] G.A. Kaminski, R.A. Friesner, J. Tirado-Rives, W.L. Jorgensen, Evaluation and reparametrization of the OPLS-AA force field for proteins via comparison with accurate quantum chemical calculations on peptides, The Journal of Physical Chemistry B 105 (2001) 6474–6487.
[27] K. Toukan, A. Rahman, Molecular-dynamics study of atomic motions in water, Physical Review B 31 (1985) 2643–2648.
[28] H.J.C. Berendsen, J.R. Grigera, T.P. Straatsma, The Missing Term in Effective Pair Potentials, Journal of Physical Chemistry 91 (1987) 6269–6271.
[29] T.A. Darden, D. York, L. Pedersen, Particle mesh Ewald: An N.log(N) method for Ewald sums in large systems, Journal of Chemical Physics 98 (1993) 10089–10092.
[30] B. Hess, H. Bekker, H.J.C. Berendsen, J.G.E.M. Fraaije, LINCS: A linear constraint solver for molecular simulations, Journal of Computational Chemistry 18 (1997) 1463–1472.
[31] T. Wiseman, S. Williston, J.F. Brandts, L.N. Lin, Rapid measurement of binding constants and heats of binding using a new titration calorimeter, Analytical Biochemistry 179 (1989) 131–137.
[32] M. Sattler, H. Liang, D. Nettesheim, R.P. Meadows, J.E. Harlan, M. Eberstadt, H.S. Yoon, S.B. Shuker, B.S. Chang, A.J. Minn, C.B. Thompson, S.W. Fesik, Structure of Bcl-xL–Bak peptide complex: recognition between regulators of apoptosis, Science 275 (1997) 983–986.
[33] A.M. Petros, E.T. Olejniczak, S.W. Fesik, Structural biology of the Bcl-2 family of proteins, Biochimica et Biophysica Acta 1644 (2004) 83–94.
[34] S. Krajewski, S. Tanaka, S. Takayama, M.J. Schibler, W. Fenton, J.C. Reed, Investigation of the subcellular distribution of the bcl-2 oncoprotein: residence in the nuclear envelope, endoplasmic reticulum, and outer mitochondrial membranes, Cancer Research 53 (1993) 4701–4714.
[35] M. Gonzalez-Garcia, R. Perez-Ballestero, L. Ding, L. Duan, L.H. Boise, C.B. Thompson, G. Nunez, Bcl-XL is the major bcl-x mRNA form expressed during murine development and its product localizes to mitochondria, Development 120 (1994) 3033–3042.
[36] H. Zha, H.A. Fisk, M.P. Yaffe, N. Mahajan, B. Herman, J.C. Reed, Structure–function comparisons of the proapoptotic protein Bax in yeast and mammalian cells, Molecular and Cellular Biology 16 (1996) 6494–6508.
[37] C.M. Dobson, Protein folding and misfolding, Nature 426 (2003) 884–890.
[38] M. Stefani, C.M. Dobson, Protein aggregation and aggregate toxicity: new insights into protein folding, misfolding diseases and biological evolution, Journal of Molecular Medicine (Berlin) 81 (2003) 678–699.
[39] M. Vendruscolo, J. Zurdo, C.E. MacPhee, C.M. Dobson, Protein folding and misfolding: a paradigm of self-assembly and regulation in complex biological systems, Philosophical Transactions. Series A, Mathematical, Physical, and Engineering Sciences 361 (2003) 1205–1222.
[40] M. Bucciantini, G. Calloni, F. Chiti, L. Formigli, D. Nosi, C.M. Dobson, M. Stefani, Prefibrillar amyloid protein aggregates share common features of cytotoxicity, Journal of Biological Chemistry 279 (2004) 31374–31382.
[41] K.K. Frousios, V.A. Iconomidou, C.M. Karletidi, S.J. Hamodrakas, Amyloidogenic determinants are usually not buried, BMC Structural Biology 9 (2009) 44.
[42] O. Conchillo-Sole, N.S. de Groot, F.X. Aviles, J. Vendrell, X. Daura, S. Ventura, AGGRESCAN: a server for the prediction and evaluation of "hot spots" of aggregation in polypeptides, BMC Bioinformatics 8 (2007) 65.
[43] B.S. Chang, A.J. Minn, S.W. Muchmore, S.W. Fesik, C.B. Thompson, Identification of a novel regulatory domain in Bcl-X(L) and Bcl-2, EMBO Journal 16 (1997) 968–977.
[44] M. Bouchard, J. Zurdo, E.J. Nettleton, C.M. Dobson, C.V. Robinson, Formation of insulin amyloid fibrils followed by FTIR simultaneously with CD and electron microscopy, Protein Science 9 (2000) 1960–1967.
[45] A. Arora, C. Ha, C.B. Park, Insulin amyloid fibrillation at above 100 degrees C: new insights into protein folding under extreme temperatures, Protein Science 13 (2004) 2429–2436.
[46] P. Juszczyk, A.S. Kolodziejczyk, Z. Grzonka, Circular dichroism and aggregation studies of amyloid beta (11-8) fragment and its variants, Acta Biochimica Polonica 52 (2005) 425–431.
[47] S. Jain, J.B. Udgaonkar, Evidence for stepwise formation of amyloid fibrils by the mouse prion protein, Journal of Molecular Biology 382 (2008) 1228–1241.
[48] E. Chatani, H. Yagi, H. Naiki, Y. Goto, Polymorphism of beta2-microglobulin amyloid fibrils manifested by ultrasonication-enhanced fibril formation in trifluoroethanol, Journal of Biological Chemistry 287 (2012) 22827–22837.
[49] G.V. Semisotnov, N.A. Rodionova, O.I. Razgulyaev, V.N. Uversky, A.F. Gripas, R.I. Gilmanshin, Study of the "molten globule" intermediate state in protein folding by a hydrophobic fluorescent probe, Biopolymers 31 (1991) 119–128.
[50] T. Ban, D. Hamada, K. Hasegawa, H. Naiki, Y. Goto, Direct observation of amyloid fibril growth monitored by thioflavin T fluorescence, Journal of Biological Chemistry 278 (2003) 16462–16465.
[51] C.M. Dobson, Experimental investigation of protein folding and misfolding, Methods 34 (2004) 4–14.
[52] S.A. Hudson, H. Ecroyd, T.W. Kee, J.A. Carver, The thioflavin T fluorescence assay for amyloid fibril detection can be biased by the presence of exogenous compounds, FEBS Journal 276 (2009) 5960–5972.
[53] A.I. Sulatskaya, I.M. Kuznetsova, K.K. Turoverov, Interaction of thioflavin T with amyloid fibrils: stoichiometry and affinity of dye binding, absorption spectra of bound dye, The Journal of Physical Chemistry B 115 (2011) 11519–11524.
[54] K. Ono, Y. Yoshiike, A. Takashima, K. Hasegawa, H. Naiki, M. Yamada, Potent anti–amyloidogenic and fibril-destabilizing effects of polyphenols in vitro: implications for the prevention and therapeutics of Alzheimer's disease, Journal of Neurochemistry 87 (2003) 172–181.
[55] M.R. Krebs, D.K. Wilkins, E.W. Chung, M.C. Pitkeathly, A.K. Chamberlain, J. Zurdo, C.V. Robinson, C.M. Dobson, Formation and seeding of amyloid fibrils from wild-type hen lysozyme and a peptide fragment from the beta-domain, Journal of Molecular Biology 300 (2000) 541–549.
[56] L.A. Morozova-Roche, J. Zurdo, A. Spencer, W. Noppe, V. Receveur, D.B. Archer, M. Joniau, C.M. Dobson, Amyloid fibril formation and seeding by wild-type human lysozyme and its disease-related mutational variants, Journal of Structural Biology 130 (2000) 339–351.
[57] F.G. De Felice, M.N. Vieira, M.N. Meirelles, L.A. Morozova-Roche, C.M. Dobson, S.T. Ferreira, Formation of amyloid aggregates from human lysozyme and its disease-associated variants using hydrostatic pressure, The FASEB Journal 18 (2004) 1099–1101.
[58] N. Arispe, H.B. Pollard, E. Rojas, beta-Amyloid Ca(2+)-channel hypothesis for neuronal death in Alzheimer disease, Molecular and Cellular Biochemistry 140 (1994) 119–125.
[59] T. Mirzabekov, M.C. Lin, W.L. Yuan, P.J. Marshall, M. Carman, K. Tomaselli, I. Lieberburg, B.L. Kagan, Channel formation in planar lipid bilayers by a neurotoxic fragment of the beta-amyloid peptide, Biochemical and Biophysical Research Communications 202 (1994) 1142–1148.
[60] Y. Hirakura, R. Azimov, R. Azimova, B.L. Kagan, Polyglutamine-induced ion channels: a possible mechanism for the neurotoxicity of Huntington and other CAG repeat diseases, Journal of Neuroscience Research 60 (2000) 490–494.
[61] Y. Hirakura, W.W. Yiu, A. Yamamoto, B.L. Kagan, Amyloid peptide channels: blockade by zinc and inhibition by Congo red (amyloid channel block), Amyloid 7 (2000) 194–199.

[62] H.A. Lashuel, D. Hartley, B.M. Petre, T. Walz, P.T. Lansbury Jr., Neurodegenerative disease: amyloid pores from pathogenic mutations, Nature 418 (2002) 291.
[63] A.J. Minn, P. Velez, S.L. Schendel, H. Liang, S.W. Muchmore, S.W. Fesik, M. Fill, C.B. Thompson, Bcl-x(L) forms an ion channel in synthetic lipid membranes, Nature 385 (1997) 353–357.
[64] T. Kaufmann, S. Schlipf, J. Sanz, K. Neubert, R. Stein, C. Borner, Characterization of the signal that directs Bcl-x(L), but not Bcl-2, to the mitochondrial outer membrane, The Journal of Cell Biology 160 (2003) 53–64.
[65] G.R. Thuduppathy, J.W. Craig, V. Kholodenko, A. Schon, R.B. Hill, Evidence that membrane insertion of the cytosolic domain of Bcl-xL is governed by an electrostatic mechanism, Journal of Molecular Biology 359 (2006) 1045–1058.
[66] G. Basanez, J. Zhang, B.N. Chau, G.I. Maksaev, V.A. Frolov, T.A. Brandt, J. Burch, J.M. Hardwick, J. Zimmerberg, Pro-apoptotic cleavage products of Bcl-xL form cytochrome c-conducting pores in pure lipid membranes, Journal of Biological Chemistry 276 (2001) 31083–31091.
[67] G. Basanez, J.C. Sharpe, J. Galanis, T.B. Brandt, J.M. Hardwick, J. Zimmerberg, Bax-type apoptotic proteins porate pure lipid bilayers through a mechanism sensitive to intrinsic monolayer curvature, Journal of Biological Chemistry 277 (2002) 49360–49365.
[68] E.A. Jonas, J.A. Hickman, M. Chachar, B.M. Polster, T.A. Brandt, Y. Fannjiang, I. Ivanovska, G. Basanez, K.W. Kinnally, J. Zimmerberg, J.M. Hardwick, L.K. Kaczmarek, Proapoptotic N-truncated BCL-xL protein activates endogenous mitochondrial channels in living synaptic terminals, Proceedings of the National Academy of Sciences of the United States of America 101 (2004) 13590–13595.
[69] P.T. Lansbury Jr., P.R. Costa, J.M. Griffiths, E.J. Simon, M. Auger, K.J. Halverson, D.A. Kocisko, Z.S. Hendsch, T.T. Ashburn, R.G. Spencer, et al., Structural model for the beta-amyloid fibril based on interstrand alignment of an antiparallel-sheet comprising a C-terminal peptide, Nature Structural Biology 2 (1995) 990–998.
[70] J.W. Kelly, Alternative conformations of amyloidogenic proteins govern their behavior, Current Opinion in Structural Biology 6 (1996) 11–17.
[71] H.A. Lashuel, S.R. Labrenz, L. Woo, L.C. Serpell, J.W. Kelly, Protofilaments, filaments, ribbons, and fibrils from peptidomimetic self-assembly: implications for amyloid fibril formation and materials science, Journal of the American Chemical Society 122 (2000) 5262–5277.
[72] R. Nelson, M.R. Sawaya, M. Balbirnie, A.O. Madsen, C. Riekel, R. Grothe, D. Eisenberg, Structure of the cross-beta spine of amyloid-like fibrils, Nature 435 (2005) 773–778.
[73] Y. Tsujimoto, J. Cossman, E. Jaffe, C.M. Croce, Involvement of the bcl-2 gene in human follicular lymphoma, Science 228 (1985) 1440–1443.
[74] Y. Tsujimoto, C.M. Croce, Analysis of the structure, transcripts, and protein products of bcl-2, the gene involved in human follicular lymphoma, Proceedings of the National Academy of Sciences of the United States of America 83 (1986) 5214–5218.
[75] S. Haldar, J.C. Reed, C. Beatty, C.M. Croce, Role of bcl-2 in growth factor triggered signal transduction, Cancer Research 50 (1990) 7399–7401.
[76] D. Hockenbery, G. Nunez, C. Milliman, R.D. Schreiber, S.J. Korsmeyer, Bcl-2 is an inner mitochondrial membrane protein that blocks programmed cell death, Nature 348 (1990) 334–336.
[77] S.J. Korsmeyer, T.J. McDonnell, G. Nunez, D. Hockenbery, R. Young, Bcl-2: B cell life, death and neoplasia, Current Topics in Microbiology and Immunology 166 (1990) 203–207.
[78] Z. Xie, S. Schendel, S. Matsuyama, J.C. Reed, Acidic pH promotes dimerization of Bcl-2 family proteins, Biochemistry 37 (1998) 6410–6418.
[79] J.W. O'Neill, M.K. Manion, B. Maguire, D.M. Hockenbery, BCL-XL dimerization by three-dimensional domain swapping, Journal of Molecular Biology 356 (2006) 367–381.
[80] S.Y. Jeong, B. Gaume, Y.J. Lee, Y.T. Hsu, S.W. Ryu, S.H. Yoon, R.J. Youle, Bcl-x(L) sequesters its C-terminal membrane anchor in soluble, cytosolic homodimers, EMBO Journal 23 (2004) 2146–2155.
[81] A. Ospina, A. Lagunas-Martinez, J. Pardo, J.A. Carrodeguas, Protein oligomerization mediated by the transmembrane carboxyl terminal domain of Bcl-XL, FEBS Letters 585 (2011) 2935–2942.
[82] P.T. Lansbury Jr., Consequences of the molecular mechanism of amyloid formation for the understanding of the pathogenesis of Alzheimer's disease and the development of therapeutic strategies, Arzneimittel-Forschung 45 (1995) 432–434.
[83] K.K. Chung, V.L. Dawson, T.M. Dawson, The role of the ubiquitin–proteasomal pathway in Parkinson's disease and other neurodegenerative disorders, Trends in Neurosciences 24 (2001) S7–S14.
[84] D.J. Selkoe, Folding proteins in fatal ways, Nature 426 (2003) 900–904.
[85] C.A. Ross, M.A. Poirier, Protein aggregation and neurodegenerative disease, Nature Medicine 10 (2004) S10–S17, (Suppl.).
[86] L.B. Dyksterhuis, E.A. Carter, S.M. Mithieux, A.S. Weiss, Tropoelastin as a thermodynamically unfolded premolten globule protein: The effect of trimethylamine N-oxide on structure and coacervation, Archives of Biochemistry and Biophysics 487 (2009) 79–84.
[87] A.L. Gharibyan, V. Zamotin, K. Yanamandra, O.S. Moskaleva, B.A. Margulis, I.A. Kostanyan, L.A. Morozova-Roche, Lysozyme amyloid oligomers and fibrils induce cellular death via different apoptotic/necrotic pathways, Journal of Molecular Biology 365 (2007) 1337–1349.
[88] R.J. Clem, E.H. Cheng, C.L. Karp, D.G. Kirsch, K. Ueno, A. Takahashi, M.B. Kastan, D.E. Griffin, W.C. Earnshaw, M.A. Veliuona, J.M. Hardwick, Modulation of cell death by Bcl-XL through caspase interaction, Proceedings of the National Academy of Sciences of the United States of America 95 (1998) 554–559.